NO_x Control Options and Integration for US Coal Fired Boilers

Quarterly Progress Report

Reporting Period Start Date January 1, 2004
Reporting Period End Date: March 31, 2004

Mike Bockelie, REI
Kevin Davis, REI
Temi Linjewile, REI
Connie Senior, REI
Eric Eddings, University of Utah
Kevin Whitty, University of Utah
Larry Baxter, Brigham Young University
Calvin Bartholomew, Brigham Young University
William Hecker, Brigham Young University
Stan Harding, N.S. Harding & Associates

April 30, 2004

DOE Cooperative Agreement No: DE-FC26-00NT40753

Reaction Engineering International
77 West 200 South, Suite 210
Salt Lake City, UT 84101

Disclaimer

“This report was prepared as an account of work sponsored by an agency of the United States Government. Neither the United States Government nor any agency thereof, nor any of their employees, makes any warranty, express or implied, or assumes any legal liability or responsibility for the accuracy, completeness, or usefulness of any information, apparatus, product, or process disclosed, or represents that its use would not infringe privately owned rights. Reference herein to any specific commercial product, process, or service by trade name, trademark, manufacturer, or otherwise does not necessarily constitute or imply its endorsement, recommendation, or favoring by the United States Government or any agency thereof. The views and opinions of authors expressed herein do not necessarily state or reflect those of the United States Government or any agency thereof.”

Abstract

This is the fifteenth Quarterly Technical Report for DOE Cooperative Agreement No: DE-FC26-00NT40753. The goal of the project is to develop cost effective analysis tools and techniques for demonstrating and evaluating low NO_x control strategies and their possible impact on boiler performance for boilers firing US coals. The Electric Power Research Institute (EPRI) is providing co-funding for this program. At AEP's Gavin Plant, data from the corrosion probes showed that corrosion rate increased as boiler load was increased. During an outage at the plant, the drop in boiler load, sensor temperature and corrosion rate could all be seen clearly. Restarting the boiler saw a resumption of corrosion activity. This behavior is consistent with previous observations made at a 600MWe utility boiler. More data are currently being examined for magnitudes of corrosion rates and changes in boiler operating conditions. Considerable progress was made this quarter in BYU's laboratory study of catalyst deactivation. Surface sulfation appears to partially suppress NO adsorption when the catalyst is not exposed to NH_3; NH_3 displaces surface-adsorbed NO on SCR catalysts and surface sulfation increases the amount of adsorbed NH_3, as confirmed by both spectroscopy and TPD experiments. However, there is no indication of changes in catalyst activity despite changes in the amount of adsorbed NH_3. A monolith test reactor (MTR), completed this quarter, provided the first comparative data for one of the fresh and field-exposed monolith SCR catalysts yet developed in this project. Measurements of activity on one of the field-exposed commercial monolith catalysts do not show significant changes in catalyst activity (within experimental error) as compared to the fresh catalyst. The exposed surface of the sample contains large amounts of Ca and Na, neither of which is present in the fresh sample, even after removal of visibly obvious fouling deposits. However, these fouling compounds do not deactivate the catalyst to the extent that these same poisons do in the deliberately wet-impregnated laboratory-prepared samples ($1\%V_2O_5$-$9\%WO_3/TiO_2$). At least in this case, the fouling deposits generated by field exposure present little if any chemical deactivation or barrier to mass transfer. During this quarter, the slipstream reactor at Rockport operated for 1000 hours on flue gas. Periodic NO_x reduction measurements were made, showing some decrease in activity relative to fresh catalyst samples. Plans are being made to take the reactor out of service at the Rockport plant and move it to Plant Gadsden. At Gadsden, inlet and outlet ports were installed on Unit 1 for the slipstream reactor during an outage.

Table of Contents

1

Executive Summary

The work to be conducted in this project received funding from the Department of Energy under Cooperative Agreement No: DE-FC26-00NT40753. This project has a period of performance that started February 14, 2000 and continues through December 30, 2004.

Our program contains five major technical tasks:

- evaluation of Rich Reagent Injection (RRI) for in-furnace NO_x control;
- demonstration of RRI technologies in full-scale field tests at utility boilers;
- impacts of combustion modifications (including corrosion and soot);
- ammonia adsorption / removal from fly ash; and
- SCR catalyst testing.

To date, good progress is being made on the overall program. We have seen considerable interest from industry in the program due to our successful initial field tests of the RRI technology and the corrosion monitor.

During the last three months, our accomplishments include the following:

For the corrosion monitoring system being tested at AEP's Gavin plant:

- Preparation and installation of software, equipment and parts to be used for resolving the problem of slag covering the face of the corrosion probe.

- Attempts were made to incorporate in the control system a means for making sure the SMC control valves are shut completely when the corrosion probe temperature drops due to slag cover. This required obtaining relays, solenoid valves and Fieldpoint attachments. These were installed in the corrosion probe control boxes in February 2004.

- Procurement of parts and repair of communication equipment for reestablishing the network communication between the corrosion probes on the boiler south wall and the host site PC.

- Commencement of analysis of available electrochemical corrosion rate data.

- Completion of analysis of October 03 – February 04 data and the writing of a paper for presentation at the 29th Clearwater Conference

- Troubleshooting and repair of damaged noise modules

Considerable progress was made this quarter in BYU's laboratory study of catalyst deactivation. Further study confirms that sulfate species do not form on vanadium sites under any conditions thus far tested and that sulfate species adsorbed on SCR surfaces convert to gas-phase compounds in the presence of NH_3 at high reaction temperatures in the absence of gas-phase SO_2. Surface sulfation appears to partially suppress NO adsorption when the catalyst is not exposed to NH_3; NH_3 displaces surface-adsorbed NO on SCR catalysts and surface sulfation increases the amount of adsorbed NH_3, as confirmed by both spectroscopy and TPD

experiments. However, there is no indication of changes in catalyst activity despite changes in the amount of adsorbed NH_3.

An investigation of intrinsic catalyst activity using powdered catalyst samples based on BYU data and on literature data highlights the impact of particle size on conversions and apparent activity. The smallest particles studied at BYU ranged from 90-106 microns in diameter and appear to be only marginally influenced by pore diffusion resistance at temperatures up to 375 °C. The effectiveness factor decreases with increasing average particle size above about 100 microns, consistent with theory. Analyses of catalysts poisoned with Na and Ca at various levels and under commercial reaction conditions provided qualitatively similar results to those reported in the literature. Quantitative comparison between the BYU results and literature results suggests that the literature data include pore diffusion effects in overall apparent activity. These conclusions assume that some of the missing details in the literature data (pore size distributions, porosity, etc.) have values similar to those for the BYU samples. These effects do not change the overall trends and can never become so limiting that kinetic activities are unimportant, but they complicate model development and other aspects of quantitative rate analysis.

A monolith test reactor (MTR), completed this quarter, provided the first comparative data for one of the fresh and field-exposed monolith SCR catalysts yet developed in this project. Measurements of activity on one of the commercial monolith catalysts (M1) indicate that after 2000 h of exposure to flue gas containing fly ash, catalyst activity does not change (within experimental error) compared to the fresh catalyst. The exposed surface of the sample contains large amounts of Ca and Na, neither of which is present in the fresh sample, even after removal of visibly obvious fouling deposits. However, these fouling compounds do not deactivate the catalyst to the extent that these same poisons do in the deliberately wet-impregnated laboratory-prepared samples ($1\%V_2O_5$-$9\%WO_3/TiO_2$). At least in this case, the fouling deposits generated by field exposure present little if any chemical deactivation or barrier to mass transfer.

Both the FTIR and the MS systems required repair this quarter and are now functional again.

During this quarter, the slipstream reactor at Rockport operated for 1000 hours on flue gas. Periodic NO_x reduction measurements were made, showing some decrease in activity relative to fresh catalyst samples. Plans are being made to take the reactor out of service at the Rockport plant and move it to Plant Gadsden. At Gadsden, inlet and outlet ports were installed on Unit 1 for the slipstream reactor during an outage.

Experimental Methods

Within this section we present in order, brief discussions on the different tasks that are contained within this program. For simplicity, the discussion items are presented in the order of the tasks as outlined in our original proposal.

Task 1 - Program Management

During the last performance period,

- Corrosion Probe:
  - Preparation and installation of software, equipment and parts to be used for resolving the problem of slag covering the face of the corrosion probe.
  - Analysis of available electrochemical corrosion rate data.
- SCR:
  - Investigation of sulfation of SCR catalyst continued.
  - A monolith test reactor (MTR), completed this quarter, provided the first comparative data for one of the fresh and field-exposed monolith SCR catalysts yet developed in this project.
  - During this quarter, the slipstream reactor at Rockport operated for 1000 hours on flue gas. Periodic NOx reduction measurements were made, showing some decrease in activity relative to fresh catalyst samples.
  - Plans are being made to take the reactor out of service at the Rockport plant and move it to Plant Gadsden. At Gadsden, inlet and outlet ports were installed on Unit 1 for the slipstream reactor during an outage.

Industry Involvement

Results from portions of this research program have been reported to industry through technical presentations at conferences. Two papers was presented at the Electric Power Conference, Baltimore, Maryland, March 30-April 1, 2004:

- Constance Senior and Temi Linjewile, “Understanding Oxidation of Mercury Across SCR Catalysts in Power Plants Burning Low Rank Coals.”
- Marc Cremer, David Wang, and Bradley Adams, "Design of Reagent Injection Systems for NO_x Control In Coal Fired Utility Boilers."

Two papers will be presented next quarter at the 29th Coal Utilization & Fuel Systems Conference in Clearwater, Florida, April 18-22, 2004:

- Kevin Davis, Temi Linjewile, David Swensen, Darrin Shino, J.J. Letcavits, William Cox and Richard Carr, “A Multi-point Corrosion Monitoring System Applied in a 1300 MW Coal-fired Boiler.”
- Constance Senior and Temi Linjewile, “Oxidation Of Mercury Across SCR Catalysts In Coal-Fired Power Plants.”

Task 3 Minimization of Impacts

Using the initial CFD baseline modeling of the Gavin Station and the plant corrosion maps, six boiler locations for the corrosion probes were identified and access ports have been installed.

Six corrosion probes operating based on electrochemical noise have been inserted into the unit. Alongside each of the electrochemical noise corrosion probes, three EPRI/KEMA screw-in type corrosion coupons (KEMCOP) have been installed. Shakedown tests have been completed; a power surge caused three of the probes to malfunction. The replacement parts have been received and additional surge protection installed on all probe electronics. The wireless data transfer between probes has been successfully demonstrated as has the software needed to perform data collection on all six probes. Further, remote monitoring of the electrochemical noise probes from REI's office in Salt Lake City, Utah, has been established.

Combustion Impacts

Electrochemical Noise Corrosion Measurements

Corrosion measurement using the EN technique and the KEMA screw-in type corrosion coupons continued during this quarter. However, in January, during routine observation of the data, it was discovered that the south wall probes were not transmitting data to the host site computer. This problem was due to a fault in the data communication switches located in the main probe control box. Replacement parts were obtained and fitted into the control box in February.

Analysis of the electrochemical noise corrosion rate data is in progress. A summary of the data collected up until February has been compiled for a paper to be presented at the 29th International Technical Conference on Coal Utilization & Fuel Systems (Clearwater Conference) in April. A copy of the paper is attached in this report as Appendix A.

Effect of Boiler Load on Corrosion Rate

The following discussion shows the behavior of the corrosion sensors at two probe locations before and after a brief outage in November, 2003. Figure 1 shows the response of the corrosion sensor at the left corner of the south wall (Probe 2) of the boiler prior to an outage. The graph shows corrosion rate, boiler load and the sensor temperature trace. As the boiler load increased, there was a corresponding increase in corrosion rate. The boiler load then stabilized, causing the probe also to reach stable operation. The ensuing drop in boiler load, sensor temperature and corrosion rate occurred during an outage. Figure 2 shows the same phenomena captured by the Main Probe located at the center of the south wall. It may be noted that the magnitude of corrosion rate at the two locations is significantly different. Restarting the boiler saw a resumption of corrosion activity. Figure 3 shows the Main Probe response as the boiler load was ramped up. Clearly, corrosion rate increased as boiler load was increased. This behavior is consistent with previous observations made at a 600MWe utility boiler. More data are currently being examined for magnitudes of corrosion rates and changes in boiler operating conditions.

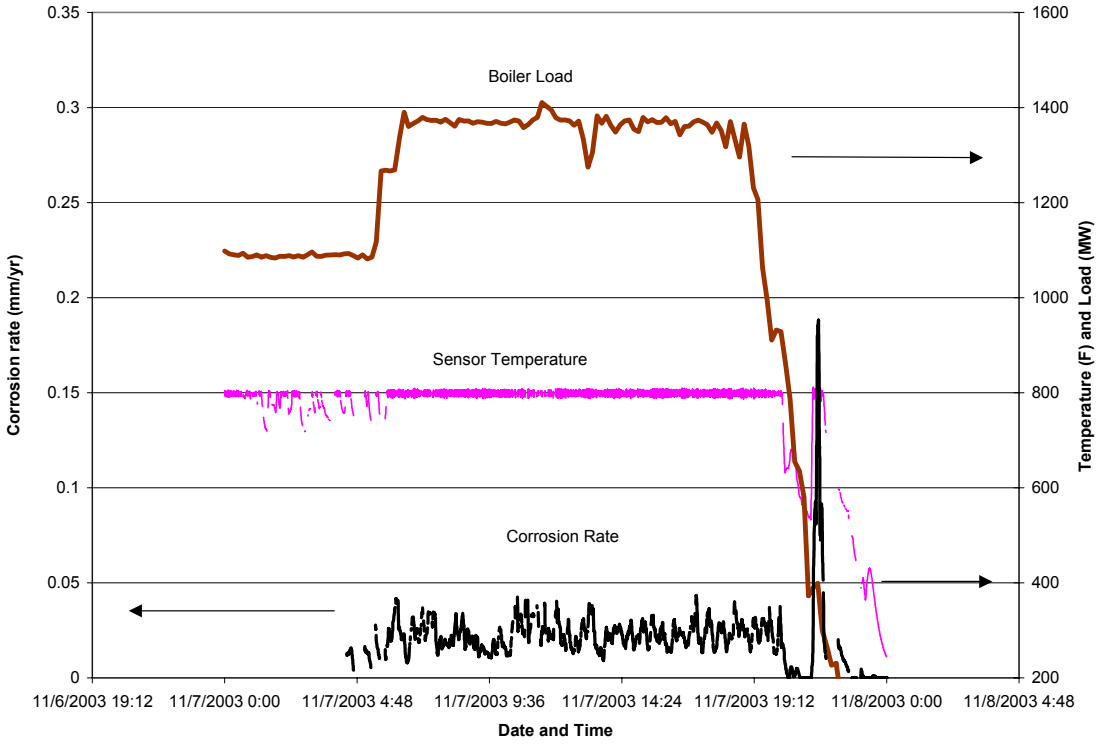

Figure 1. Electrochemical noise sensor (Probe 2) response to a drop in boiler load.

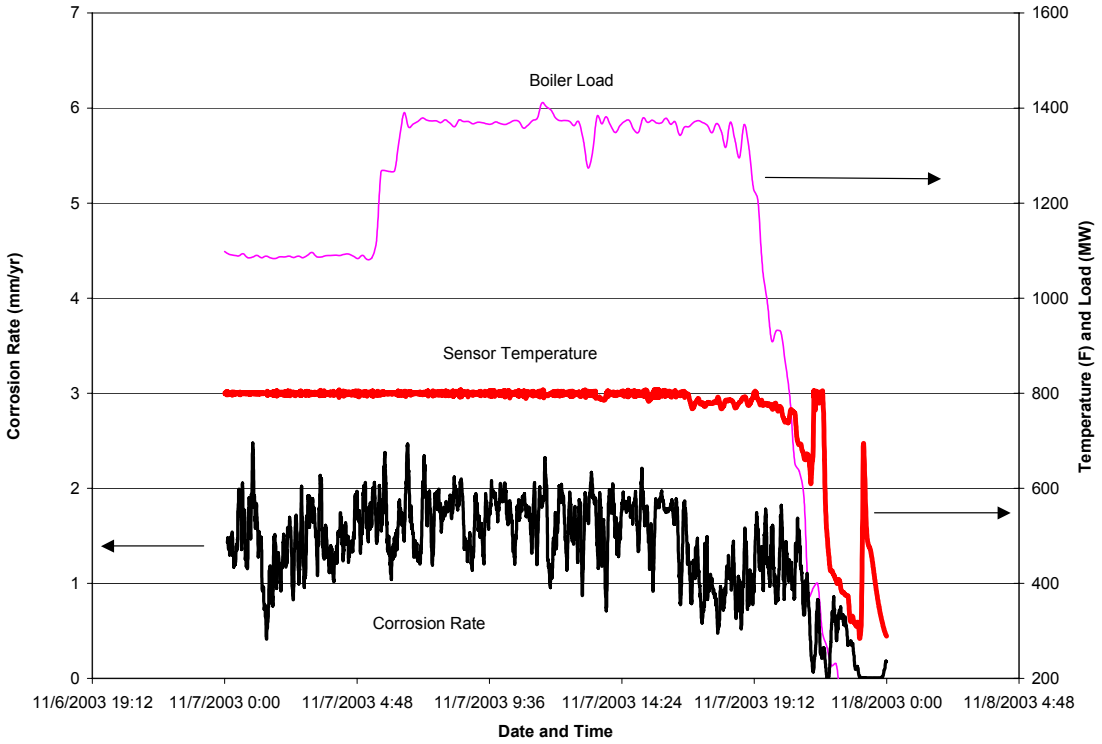

Figure 2. Electrochemical noise sensor (Main Probe) response to a drop in boiler load.

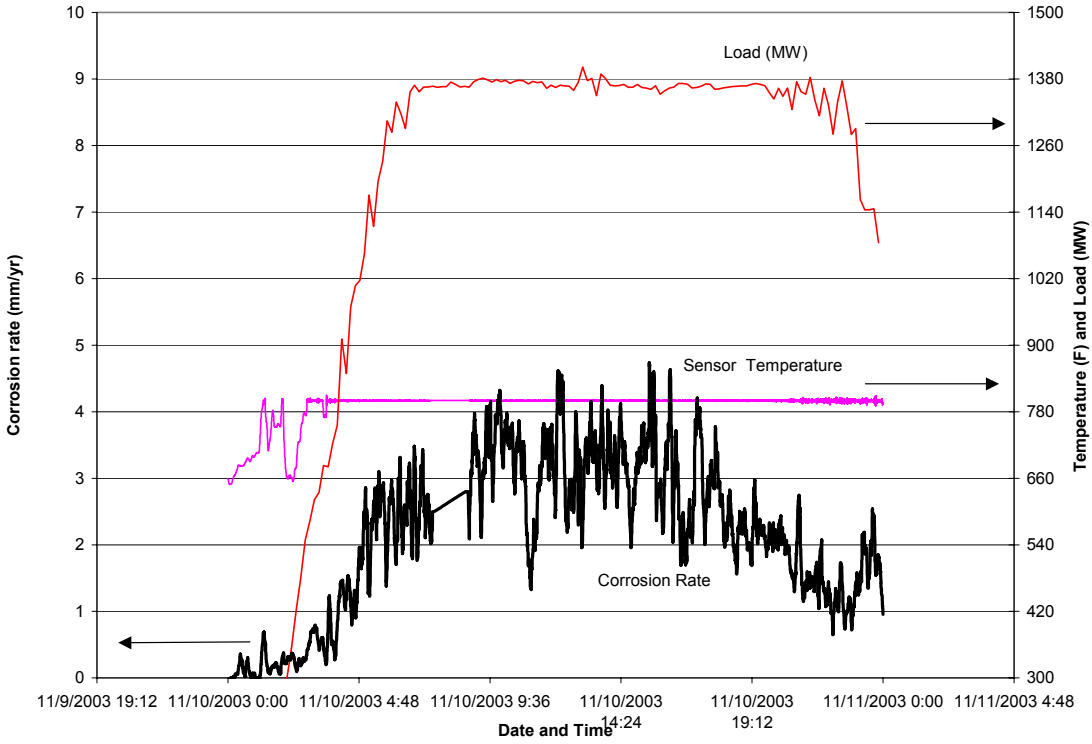

Figure 3. Effect of increasing boiler load on corrosion rate for the Main Probe.

Figures 4 and 5 show examples of selected data collected in March from the Main Probe, Probe 3 and Probe 5. During the reporting period, the Main Probe (Figure 4) showed higher corrosion rates than the other probes. Figure 4 also shows that in the first half of the week of March 22 – 28, 2004, the sensor temperature was largely below the set point value of 800°F. Since the boiler load remained mostly steady except for brief periods of low-load operation, the low sensor temperature is attributable to a dry slag deposit on the sensor elements, which insulated the sensor from radiant heat from the furnace. Further, as expected, corrosion rate during the period when the sensor temperature was below 400°F remained insignificant. It may be noted that in spite of installation of solenoid valves in the last reporting period to minimize sensor cooling during slag cover, the sensor still cooled to temperatures below 400°F. Figure 5 shows corrosion rates from Probe 3 during the period of March 1 – 7, 2004. At the end of that week there was an outage exhibited by the reduction in boiler load and sensor temperature.

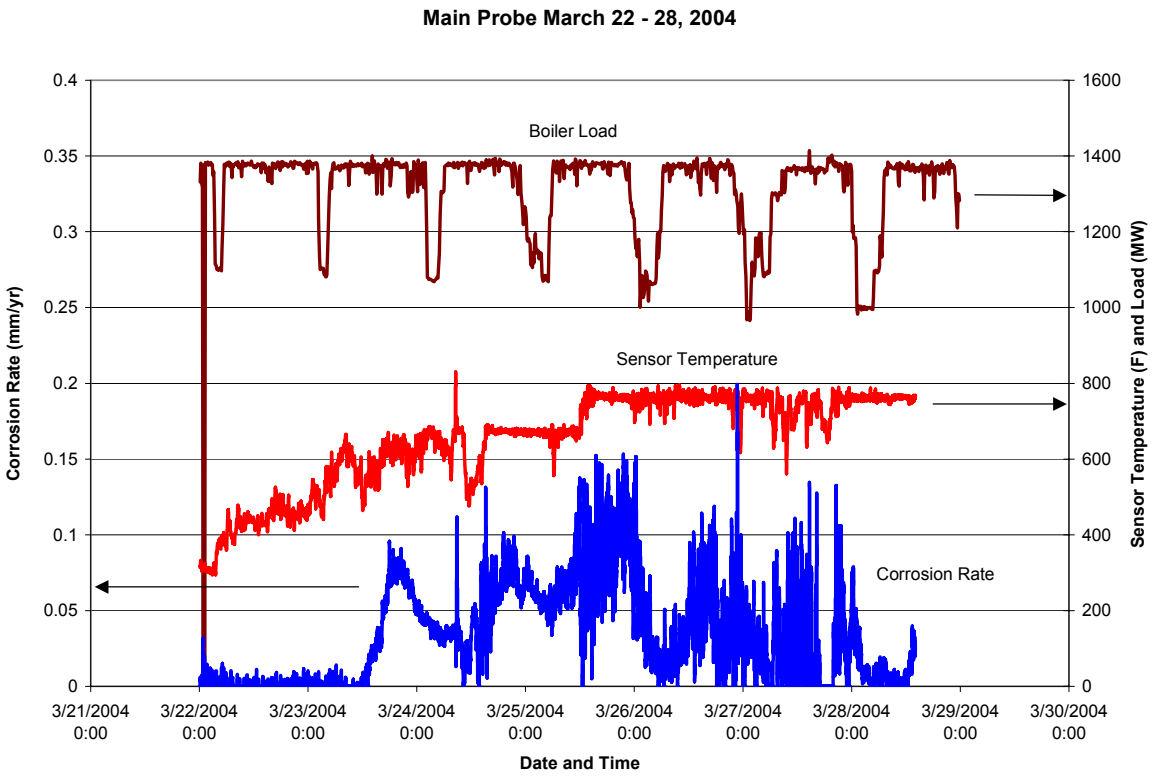

Figure 4. Sensor response for the Main Probe located on the south wall.

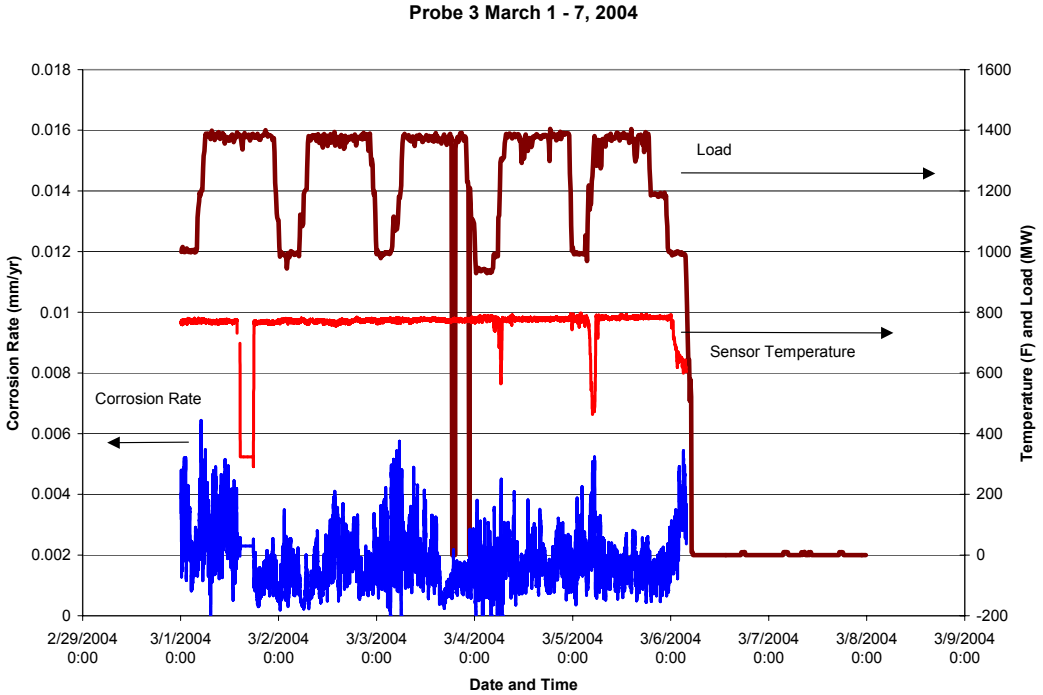

Figure 5. Corrosion sensor response for Probe 3.

Problems In The Reporting Period

Slag deposits and sensor temperature control

During this period we continued to see sensor temperature cooling down considerably due to slag cover in spite of efforts to provide a solenoid valve that shuts-off cooling air to the probe completely. Obviously a different approach is needed to alleviate the problem. Currently we have been working with the plant personnel to occasionally push the probe in and out to help clear the slag cover in the probe port.

Status of Probe 2

After an outage that occurred in the week of March 1 – 7, 2004 Probe 2 lost its ability to control temperature. At one stage the probe temperature shot up to approximately 1900°F. A temperature excursion on Probe 2 has been observed previously following an outage. It is not known why this behavior is specific to Probe 2 location.

Probe 3 EN Voltage

After the outage discussed above, Probe 3 corrosion voltage signal stopped fluctuating as it should, but instead remained constant at –5V. This behavior remained unresolved throughout this reporting period. In the past this type of behavior was caused by the sensor elements becoming "charged". In the next plant visit measures will be taken to allow remote discharging of the sensor plates should this problem occur.

Task 4 - SCR Catalyst Testing

Selective catalytic reduction (SCR) represents the only commercially proven technology capable of achieving the relatively large NO_x reductions required to comply with the latest (amended) Clean Air Act requirements. SCR systems are being installed in most large-scale utility boilers. However, most long-term experience with SCR comes from Germany and Japan and most of this is based on high-rank coal combustion. Less experience with low-rank, subbituminous coals specifically Powder River Basin coals, appears in the literature. The literature also provides essentially no US and little foreign experience with systems co-fired with biomass. The purpose of this task is to provide both laboratory and field slip steam data and analyses, including computer models, that fill this information gap.

Within this task there are for principal sub-tasks:
1. technology assessment and fundamental analysis of chemical poisoning of SCR catalysts by alkali and alkaline earth materials;
2. evaluation of commercial catalysts in a continuous flow system that simulates commercial operation;
3. evaluating the effectiveness of catalyst regeneration; and
4. develop a model of deactivation of SCR catalysts suitable for use in a CFD code.

Items 1 and 3 are principally performed at Brigham Young University (BYU) under the direction of Profs. Larry Baxter, Calvin Bartholomew, and William Hecker. The work effort for items 2 and 4 is being performed by REI, with assistance from the University of Utah and BYU. Progress during the last performance period on this task is described below.

Task 4.1 Technology Assessment/Fundamental Analysis

The objectives of this subtask are (1) to supplement the SCR-catalyst-deactivation literature with results from new laboratory-scale, experimental investigations conducted under well-controlled and commercially relevant conditions in the presence of SO_2, and (2) to provide a laboratory-based catalyst test reactor useful for characterization and analysis of SCR deactivation suitable for samples from commercial facilities, slipstream reactors, and laboratory experiments. Two catalysts flow reactors and several additional characterization systems provide the analytical tools required to achieve these objectives. The flow reactors include the *in situ* surface spectroscopy reactor (ISSR) and the catalyst characterization system (CCS), both of which are described in more detail in previous reports. Additional characterization systems include a temperature-programmable surface area and pore size distribution analyzer, scanning electron microscopes and microprobes.

The sample test matrix includes two classes of catalysts: commercial, vendor-supplied SCR catalysts and research catalysts synthesized at BYU. The commercial catalysts provide immediate relevance to practical application while the research catalysts provide unfettered ability to publish details of catalyst properties. The five commercial catalysts selected for use come from most commercially significant catalyst manufacturers (Cormetech, Haldor-Topsoe, Hitachi, and Siemens) and provide a wide range of catalyst designs and compositions. The in-

house catalysts will be subjected to detailed analysis, activity testing, and characterization, thus providing a comprehensive test and analysis platform from which to determine rates and mechanisms of catalyst deactivation. The result of this task will be a mathematical model capable of describing rates and mechanisms of deactivation.

Within the last performance period, *in situ*, spectroscopic experiments partially reported last quarter were completed. The most significant finding of these investigations is a consistent indication that vanadium does not sulfate during SCR activity in the presence of gas-phase SO_2 while both the substrate (anatase) and modifiers (molybdenum) do. In addition, mass-spectroscopy-based analyses of product gases from this reactor system help elucidate fundamental kinetics and deactivation mechanisms.

Sulfation study

The objective of this study is to determine the effects of sulfur compounds on catalyst activity, reaction kinetics and deactivation behavior of V_2O_5/TiO_2 for SCR applications in coal and biomass combustion. The motivation for this work can be summarized as follows:

1. Most ash-derived contaminants and oxide components of the catalyst experience relatively high SO_2 concentrations when used in coal-fired combustors. Most of these compounds form basic sulfates. The literature is in unanimous agreement that SCR catalytic activity arises from the acidity of the surface, although there remains some disagreement about the details of this acidity. Therefore, sulfate formation or deposition on a catalyst surface may profoundly affect surface acidity and hence activity. The potential sulfation of the surface represents a distinguishing characteristic of SCR catalysis in coal-fired systems and the potential formation of basic sulfates, especially from alkali and alkaline earth elements, represents a distinguishing characteristic of SCR use in low-rank-coal-fired and biomass-fired or co-fired systems.

2. Most studies have been conducted either in the absence of SO_2 or under conditions and/or durations unfavorable for sulfate formation. Most such studies appropriately mimic natural-gas-fired systems, where NO_x control commonly uses SCR. However, it is questionable if these studies are relevant to "realistic" industrial conditions involving long exposures to SO_2 in the presence of water.

3. There are conflicting views in the literature as to whether vanadium species on the catalyst surface are sulfated or not. Sulfation of the catalyst has the potential of changing the activity, the rates, and the mechanisms of the catalyst relative to non-sulfated systems.

ISSR Overview

The purpose of the FTIR-ISSR is to provide definitive indication of surface-active species through *in situ* monitoring of infrared spectra from catalytic surfaces exposed to a variety of laboratory and field conditions. The ISSR provides *in situ* transmission FTIR spectra of SO_2, NH_3, and NO_x, among other species. Absorption and desorption behaviors of these and other species are monitored. Quantitative indications of critical parameters, including Brønsted and

Lewis acidities on fresh and exposed catalysts, are included. Indications of coadsorption of NH_3 and NO_x help elucidate mechanisms and rates of both reactions and deactivation.

Instrument repair

The Fourier Transform Infrared (FTIR) spectrometer IR source power supply failed on January 19, 2004. The manufacturer-supplied replacement power supply was incompatible with our system. The manufacturer suggested updating the entire system power supply with the newest version at an approximate cost of $10,000. The problem was fixed instead with assistance from BYU instrument shop and the FTIR resumed normal operation on March 01, 2004.

The mass spectrometer (MS) system failed on November 11, 2003 due to a dirty ion source. One of the two filaments broke during removal for cleaning. Upon the suggestion of the BYU Chemistry Department, the broken filament was sent to Scientific Instrument Service for repair; however, the repaired filament failed, probably because the filament coating was too thick. Moreover, the manufacturer recommended using a new filament because there was no guarantee that the resistance and voltage of a fixed filament would work. Therefore, we ordered a new ion source (filament) and the old filament was sent back again for repair. The old filament successfully worked after two repairs and the new filament arrived and also works. The MS became operational again on February 14, 2004, although it had a leak and NO detection limit problems, both of which have since been resolved.

Surface Sulfate stability test

Twenty-four-hour sulfation tests on TiO_2, 2% V_2O_5/TiO_2, 5% V_2O_5/TiO_2 reported in the previous quarter concluded that sulfate species do not form on vanadium sites. XPS analyses conducted this quarter further confirm this conclusion as shown by data in Figure 6.

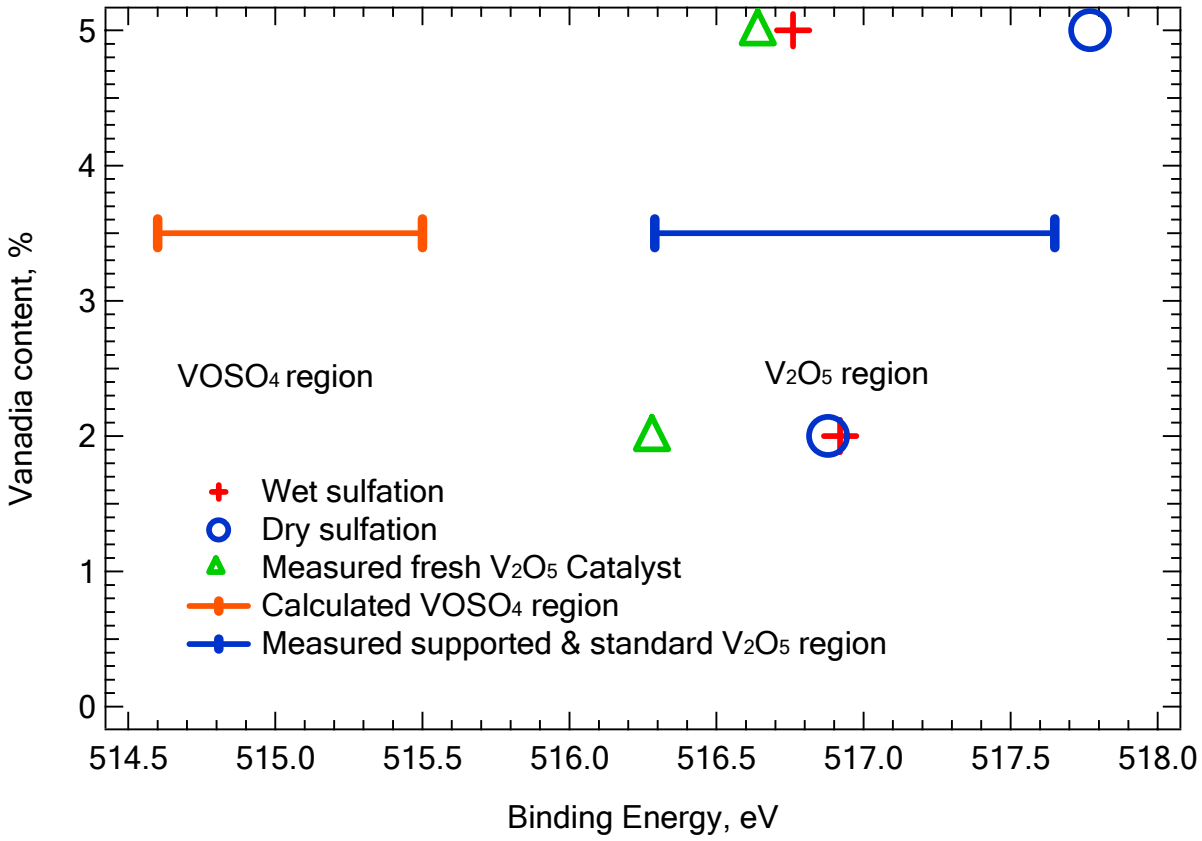

Figure 6. XPS binding energies for wet and dry sulfated vanadia catalysts.

Vanadium in an unsulfated SCR catalyst exists as vanadia, or vanidum pentoxide (V_2O_5) with vanadium in a +5 oxidation state. Thermochemical equilibrium predictions suggest that vandadium in the presence of gas-phase SO_2 forms vanadyl sulfate ($VOSO_4$) in which the oxidation state of vanadium is +4. Vandadium sulfate ($V(SO4)_2$), predicted to exist at higher temperatures in the presence of gas-phase SO_2 also includes vanadium in the +4 oxidation state. Therefore, all reasonably expected sulfation products of vanadium pentoxide reduce the vanadium oxidation state from +5 to +4.

X-ray photon spectroscopy (XPS) measures surface composition and oxidation state, the latter being measured in terms of binding energy. XPS results (Figure 6) from catalysts exposed to SO_2 under commercially relevant conditions indicate that both 2% and 5% vanadia catalysts, whether sulfated under dry or wet conditions, include vanadium in a +5 oxidation state, consistent with the spectroscopy-based conclusion that the catalyst does not sulfate reported last quarter.

The existence of the surface vanadium in a non-equilibrium state is not surprising for several reasons. These include: (1) the system is actively reacting and therefore clearly not in equilibrium, although it could possible be in local equilibrium; (2) the thermochemical properties used to predict the equilibrium condition are based on bulk samples – small surface grains introduce forces on the compounds that can and commonly do shift equilibrium from the bulk condition; and (3) the accuracy of the predictions does not include non-ideal interactions or other features that could compromise its accuracy.

Subsequent NH_3 adsorption tests on sulfated samples indicated that sulfate species on TiO_2, 2% V_2O_5/TiO_2, and 5% V_2O_5/TiO_2 surfaces were converted or removed by NH_3 at 380 ˚C. In order to find out whether sulfate remains on the surface under SCR conditions, SCR gases (1000 ppm for each of NH_3, NO and SO_2, 5% O_2, and He balanced with water vapor) were passed through sulfated TiO_2, 2% and 5% V_2O_5/TiO_2 at 380 ˚C. Since the FTIR was nonfunctional during the experiment, only XPS data could be collected which show that sulfated species remain on TiO_2 and V_2O_5/TiO_2 surfaces during SCR conditions at 380 ˚C.

NO adsorption test

While our data indicate in several independent ways that vanadium does not sulfate on SCR surfaces, gas-phase SO_2 nevertheless affects surface chemistry. This is illustrated in a series of NO adsorption tests. In the first test, a TiO_2 sample pre-sulfated for twenty-four hours was exposed to two gas environment, one containing 1900 ppm NO and 9.5% O_2 (He balance) and the second containing no NO. Both exposures were at room temperature since NO adsorption has previously been reported to decrease with increasing sample temperature. As illustrated in Figure 7, NO did not adsorb on this surface, as indicated by no spectral absorption peak near 1630 cm^{-1} in these pure titania data. A difference spectrum is also included in which it is clear that nothing adsorbed on the surface with the introduction of NO. The spectra in this and all other similar figures are offset along the ordinate so they can be clearly seen. Also, only every two-hundredth data symbol has been included on the lines so the values are not obscured by excessive numbers of symbols.

By contrast, a similar but lightly sulfated 2% V_2O_5/TiO_2 sample generated at 380 ˚C in a reactant gas containing SO_2 produced a pronounced NO adsorption peak (Figure 8). Sulfation of this sample was so minimal that XPS spectroscopy results did not detect any sulfur, probably due to its limited sensitivity (detection limit of approximately 1%). TOFSIMS analyses confirmed the presence of low-levels of sulfur on the surface. In this comparison, fresh and lightly sulfated 2% V_2O_5/TiO_2 catalysts were exposed at room temperature to a gas containing 1000 ppm NO, 5% O_2 (He balance). The IR spectra of NO adsorption on fresh and lightly sulfated 2% V_2O_5/TiO_2 are compared in Figure 8. NO adsorbed on both samples as indicated by IR peaks around 1629 cm^{-1}. Comparison of intensities of NO adsorption on fresh and lightly sulfated 2%V_2O_5/TiO_2 shows that sulfates on the surface partially suppress NO adsorption, as perhaps most evident in the difference spectrum. Incidentally, the peaks around 1498 cm^{-1} and the broad rise near 3300 cm^{-1} arise from water and possibly other impurities in the IR windows, as was verified later by IR transmission tests on the windows alone.

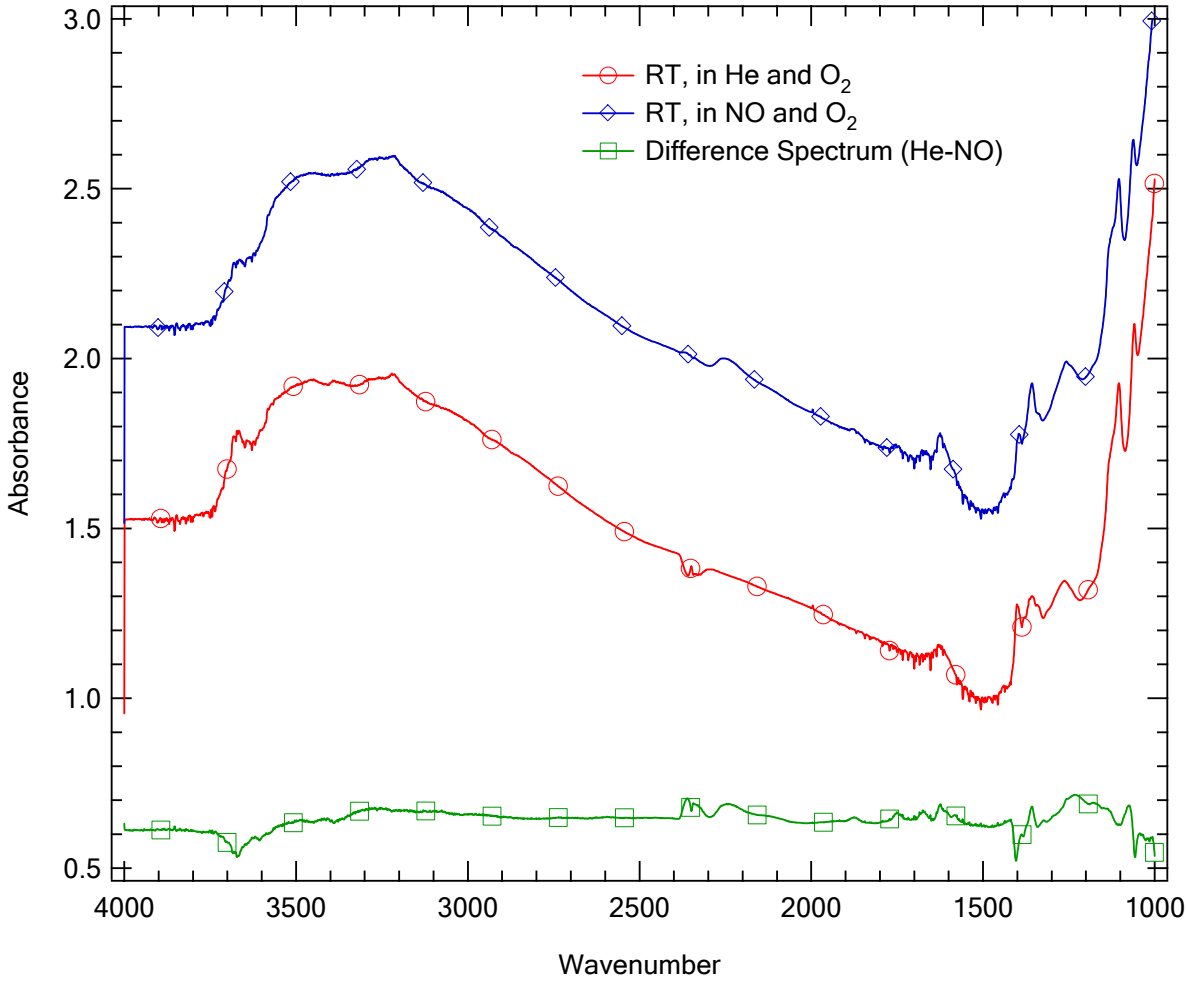

Figure 7. **NO adsorption on sulfated TiO_2, lightly sulfated and fresh 2% V_2O_5/TiO_2.**

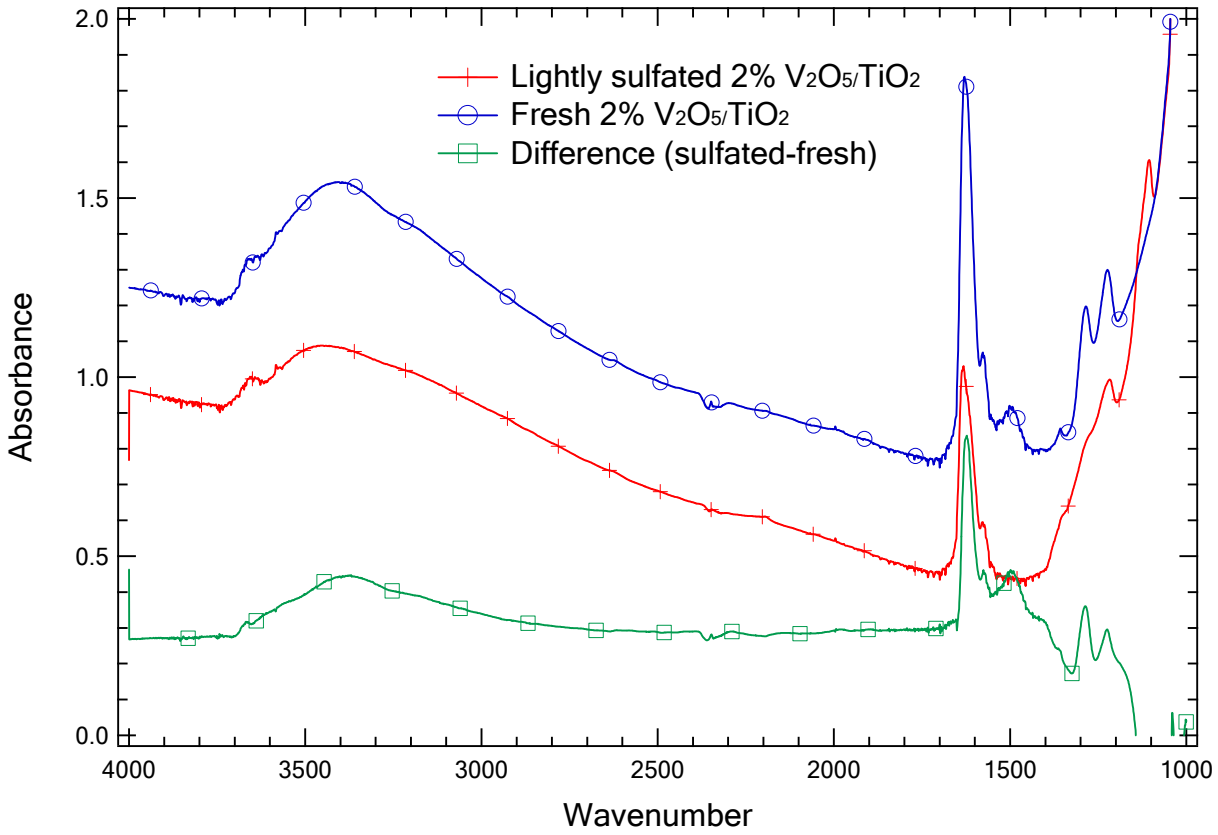

Figure 8. FTIR spectra of fresh and lightly sulfated 2% V_2O_5/TiO_2 SCR catalyst exposed to NO-containing gases. The spectra indicate the presence of surface adsorbed NO (peak at 1630 cm^{-1}).

The conclusion from these experiments is that vanadium sites do not sulfate and titanium sites do not adsorb NO. However, vanadium sites do adsorb NO and titanium sites do sulfate. Furthermore, the sulfation of titanium sites decreases the amount of NO that adsorbs on vanadium sites, indicating clear interactions between the catalytic vanadium sites and the substrate.

NO + NH_3 co-adsorption on fresh and barely sulfated 2% V_2O_5/TiO_2

NO adsorption tests reveal clear indications of NO surface chemistry. However, at SCR temperatures, our data and that in the literature agree that NO adsorption on surfaces is minimal or non-existent. Ammonia, however, does adsorb on the surface. Therefore, we conducted ammonia adsorption tests similar in concept to the NO adsorption tests described above.

In the ammonia adsorption tests, 1000 ppm NH_3 was added to 1000 ppm NO, 5% O_2 (balance He). Initially, no NH_3 adsorption could be detected by IR in these time-resolved experiments, but gradually an NH_3 adsorption peak appeared and grew more intense while the NO adsorption peak (~1627 cm^{-1}) decreased in intensity and finally disappeared. Eventually only the NH_3 adsorption peak (~1432 cm^{-1}) could be observed as shown in Figure 9 and Figure 10.

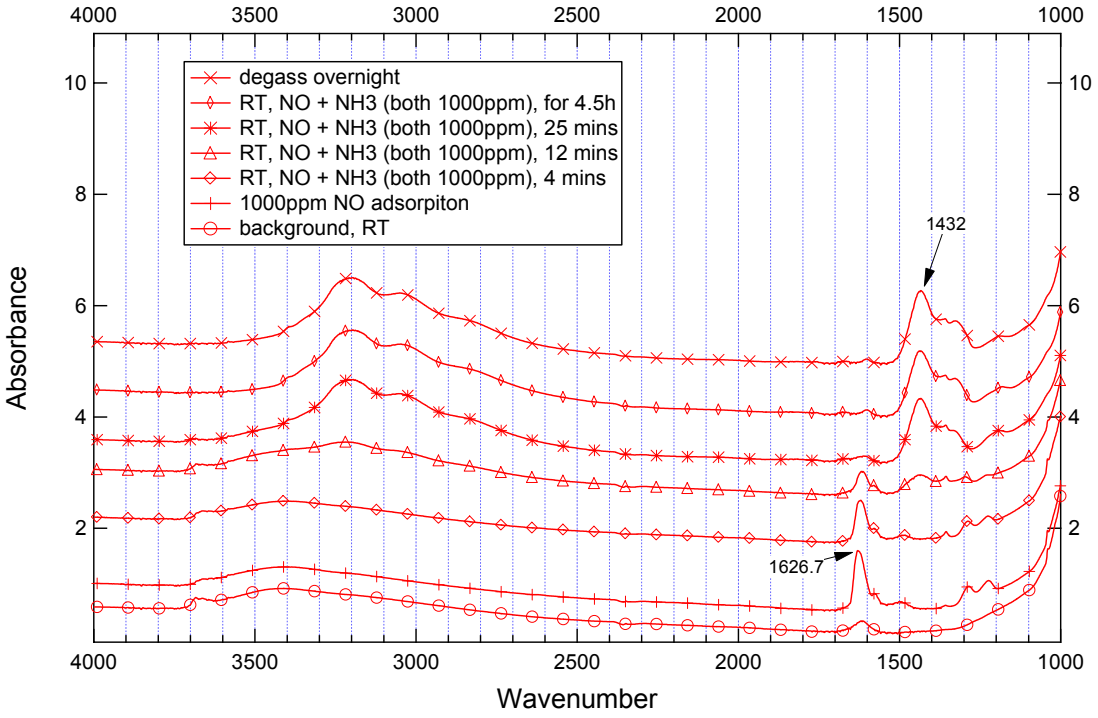

Figure 9. NO + NH_3 co-adsorption on fresh 2% V_2O_5/TiO_2 at room temperature.

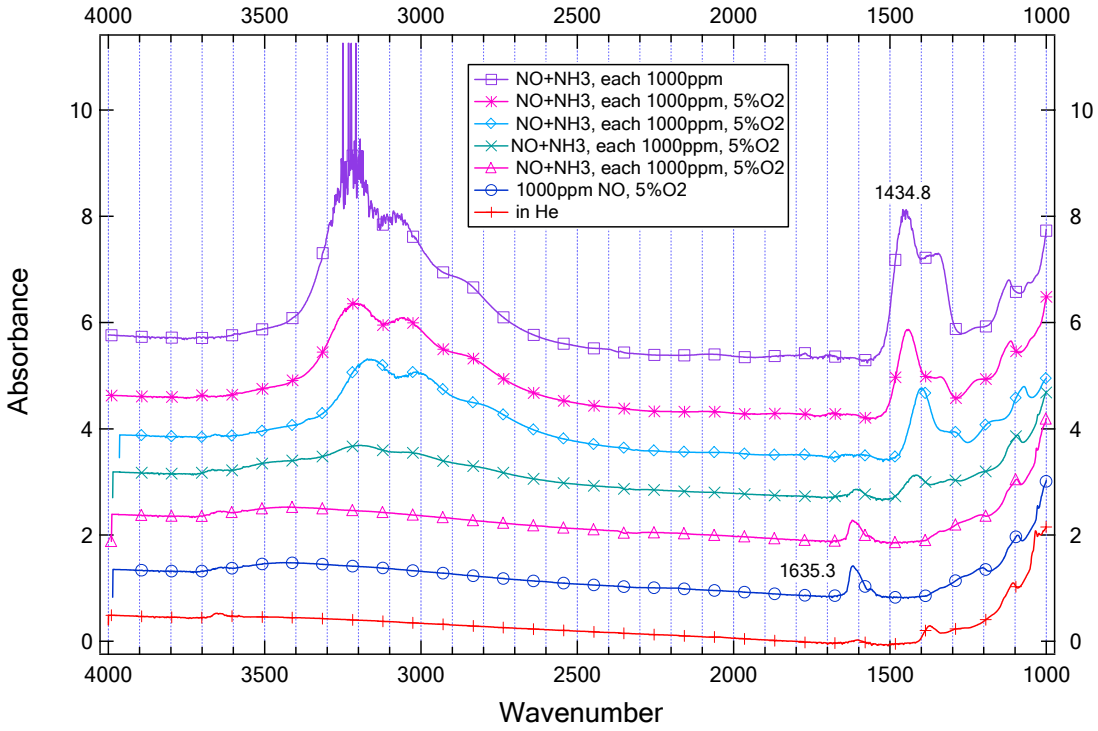

Figure 10. NO + NH_3 co-adsorption on lightly sulfated 2% V_2O_5/TiO_2 at room temperature.

In contrast to the NO adsorption experiments, in which sulfation was found to suppress the surface adsorbed NO, these ammonia adsorption experiments indicate that sulfation substantially increases the amount of adsorbed ammonia on 2% V_2O_5/TiO_2. Stronger adsorption peaks indicate that the amount of NH_3 on lightly sulfated 2% V_2O_5/TiO_2 increases, whereas a shift in the peak position toward higher wavenumbers suggests more strongly adsorbed ammonia. Both of these trends are evident here, but the dominant trend is the increased intensity (amount of adsorbed ammonia). This likely arises from increasing the number of Brønsted acid sites on the catalyst surface (either on titania sites or on the perimeter of vanadia sites or interface between vanadia and titania sites) introduced by the surface sulfated species.

The following preliminary NH_3 TPD also verifies this point.

NH_3 TPD study on fresh and barely sulfated 2% V_2O_5/TiO_2

Temperature programmed desorption (TPD) of ammonia previously adsorbed at a concentration of 1000 ppm at 25 ˚C was conducted at 5 ˚C /min from 25 ˚C to 400 ˚C on both fresh and lightly sulfated 2% V_2O_5/TiO_2 (see Figures 11 and 12). The noisy signal can be attributed to the less than optimum mass spectrometer settings; a problem that has since been corrected.

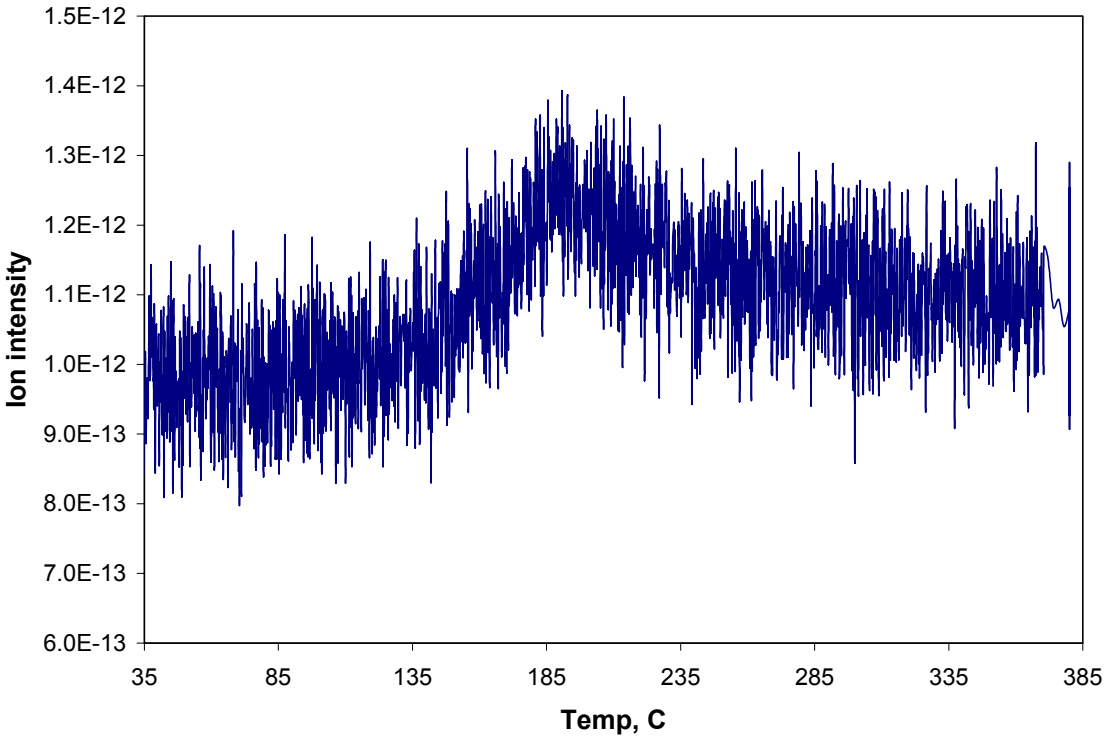

Figure 11. NH_3 TPD on lighlty sulfated 2% V_2O_5/TiO_2.

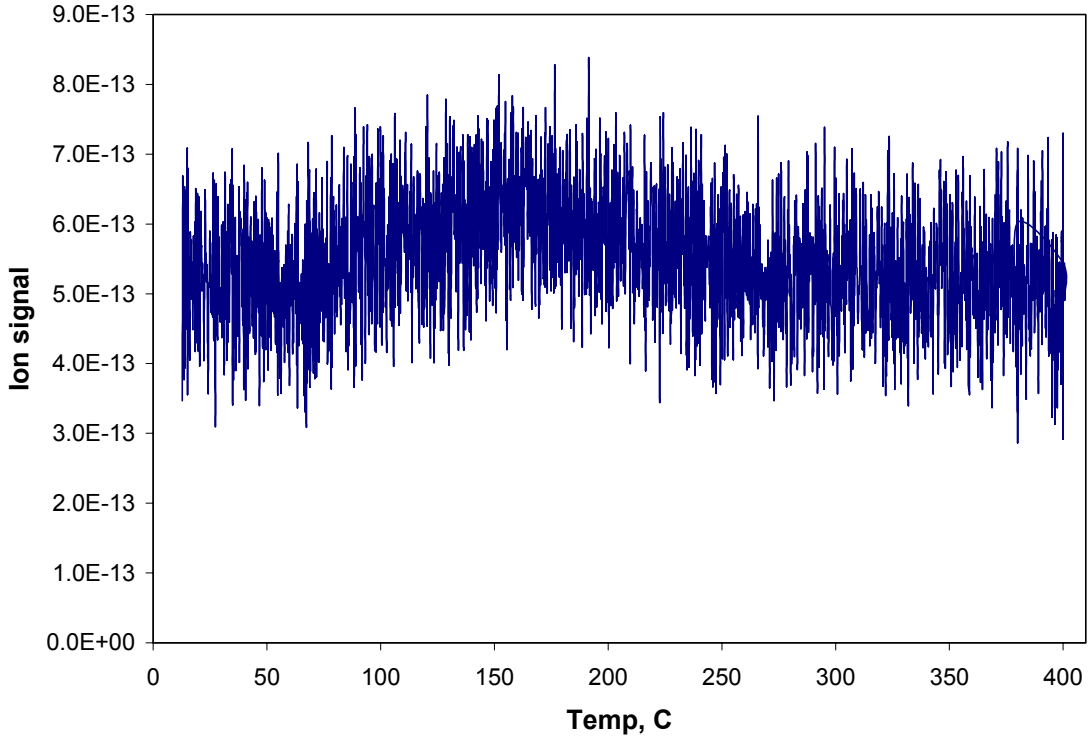

Figure 12. NH_3 TPD on fresh 2% V_2O_5/TiO_2.

The results from Figure 11 and Figure 12 show that significantly more NH_3 is desorbed from lightly sulfated 2% V_2O_5/TiO_2 than from fresh 2% V_2O_5/TiO_2. The NH_3 desorption temperature is also slightly higher for lightly sulfated 2% V_2O_5/TiO_2 (150-250 ˚C), with desportion peaking at about 200 ˚C. In the case of fresh V_2O_5/TiO_2, NH_3 desorption starts around 100 ˚C and ends up around 200 ˚C, peaking at about 185 ˚C. This difference indicates that sulfation increases the strength of NH_3 adsorption on the catalyst surface, however the dominant impact is the amount of adsorption.

Future NH_3 TPD measurements will be conducted in our TPD system in a sample cell specifically designed for TPD (rather than the IR cell), and a standard procedure is being designed.

SCR activity tests on sulfated TiO_2, fresh and lightly sulfated 2% V_2O_5/TiO_2

The gas composition for SCR activity tests in the ISSR included 1000 ppm NO, 1000 ppm NH_3, 1000 ppm SO_2, 5% O_2, and balance either wet or dry He (both wet and dry experiments are reported).

Activity was tested conducted at room temperature, 120, 200, 300, and 380 ˚C and the results indicated no activity on pure titania. An additional test with a gas containing only 1000 ppm NH_3, 1000 ppm NO, 5% O_2, and the balance He was introduced to the same TiO_2 sample at 380 ˚C; still no activity was observed.

The gas composition for SCR activity test on fresh and barely sulfated 2% V_2O_5/TiO_2 was 1000 ppm NH_3, 1000 ppm NO, with or without 1000 ppm SO_2, 5% O_2, and the balance He. All of these experiments were conducted with no water in the reactant stream. Activity was tested at

380 ˚C. The MS results from these tests are shown in Figure 13. “Out” on the top of the graph represents the MS signal from the outlet of FTIR cell, “In” represents the MS “signal from inlet of FTIR cell. It was found that MS detected the NO signal much faster than it did the SO_2 signal, which explains the greater fluctuation in the NO signal. This problem has since been fixed.

Upon addition of SO_2 to the reactant gas, no conversion of NO was observed. However, NO started to react after the SO_2 flow was stopped. This observation could be explained by inhibition of NO adsorption by SO_2. In the activity test of fresh 2% V_2O_5/TiO_2, no SO_2 was introduced; the larger differences in NO IN and OUT MS signals shown in Figure 14 indicates that NO conversion on the unsulfated catalyst is higher than on the lightly sulfated catalyst.

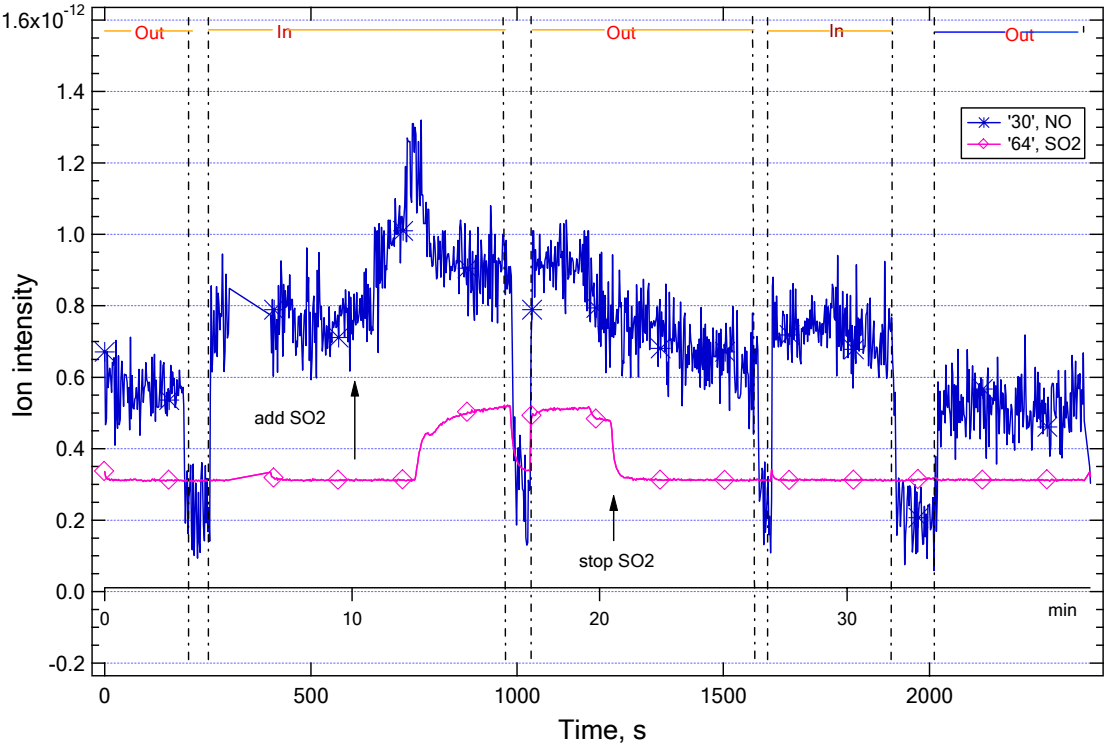

Figure 13. NO and SO_2 MS signals during SCR on lightly sulfated 2% V_2O_5/TiO_2 at 380 ˚C, showing effects of SO_2 on NO conversion.

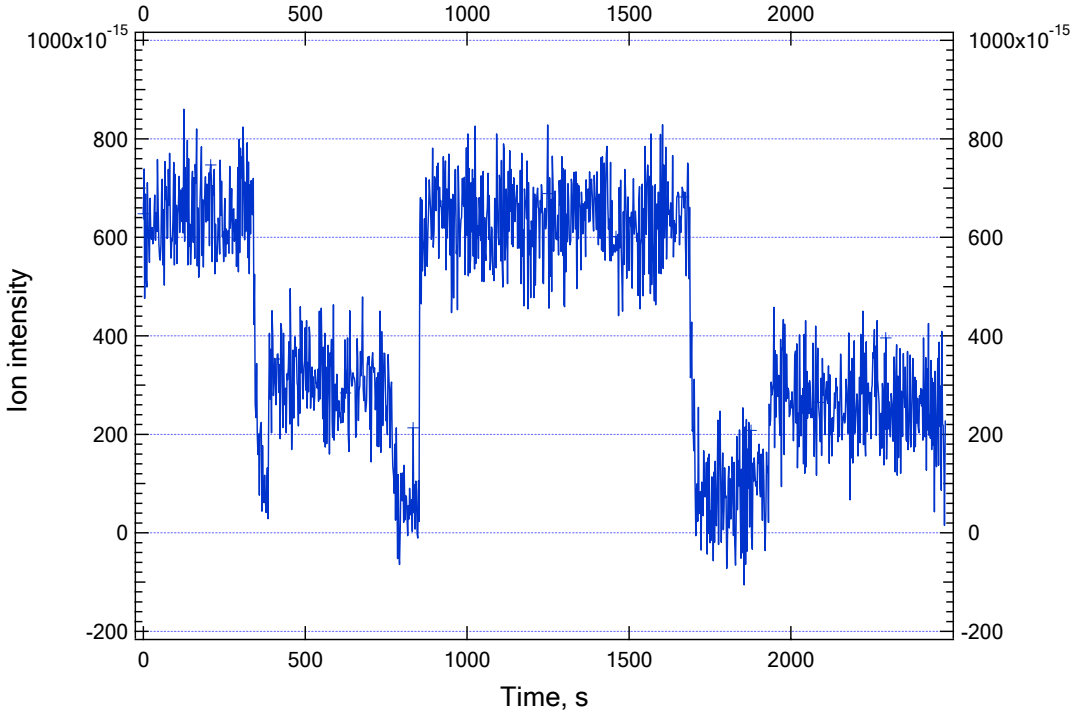

Figure 14. NO MS signals during SCR on fresh 2% V_2O_5/TiO_2 at 380 ˚C.

NO conversions under SCR conditions without gas-phase SO_2 present on fresh and lightly sulfated 2% V_2O_5/TiO_2 at 380 ˚C is compared in Table 1 and Figure 15

Table 1. Comparison of NO conversion.

2% V_2O_5/TiO_2	NO conversion
fresh	82%
lightly sulfated	42%

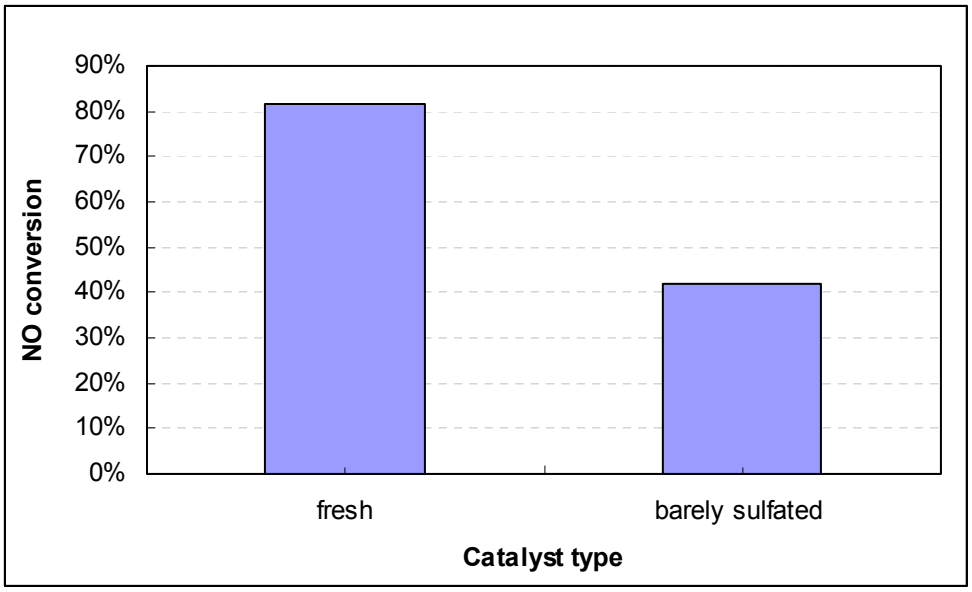

Figure 15. NO conversions for fresh and lightly sulfated V_2O_5/TiO_2.

It is apparent that the fresh 2% catalyst is a factor of two more active than the barely sulfated catalyst. However, subsequent experimentation (to be reported next quarter) reveals that this difference arises from sample preparation rather than actual catalytic activity differences.

Powdered catalyst work

CCS Overview

The catalyst characterization system (CCS) provides capabilities for long-term catalyst exposure tests required for ascertaining deactivation rates and mechanisms and a characterization facility for samples from the slipstream reactor to determine changes in reactivity and responses to well-controlled environments. This system simulates industrial flows by providing a test gas with the following nominal composition: NO, 0.1%; NH_3, 0.1%; SO_2, 0.1%; O_2, 2%; H_2O, 10%; and He, 87.7%. Both custom and commercial catalysts are tested as fresh samples and after a variety of laboratory and field exposures under steady conditions.

The CCS enables quantitative study of deactivation mechanisms by enabling measurement of specific, intrinsic catalyst reactivity of custom (laboratory) and commercial catalysts under a variety of conditions. These catalysts are impregnated with a variety of contaminants, including Ca, Na, and K. In addition, the CCS characterizes samples of catalyst from slipstream field tests to determine similar data and changes in characteristics with exposure. Advanced surface and composition analyses are used to determine composition, pore size distribution, surface area, and surface properties (acidity, extent of sulfation, etc.).

Particle size effects

In previous quarterly reports, results of a poisoning study of Ca-impregnated V_2O_5/TiO_2 catalysts were presented. The data indicate that calcium appears to *increase* catalyst activity at an

intermediate Ca:V ratio (see Figure 16, which shows NO conversion vs. Ca:V ratio both with and without SO_2 pretreatment). These observations contradict the results of previous research where activity was found to decrease monotonically with increase poison concentration (Chen, Buzanowski *et al.* 1990; Chen and Yang 1990).

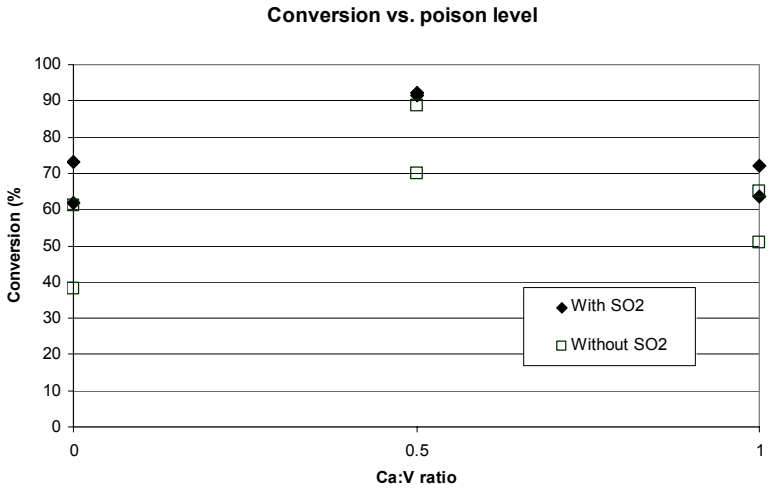

Figure 16. Conversion vs. Ca:V ratio.

In our previous study, catalyst particles were ground to a powder, and were assumed to be small enough to be essentially free of pore diffusion effects. Although the large part of our catalyst consisted of powder (generally less than 100 microns), there were possibly larger catalyst granules in which reaction rates would have been reduced by pore diffusion. It is also possible that a non-homogeneous mixture of particles of various sizes resulted in different patterns of gas flow, including channeling through the packed catalyst bed.

Furthermore, differences in catalyst granule size and packing may have caused the observed large variations in pressure drop among runs (from ~0.5 to 5.6 psig). Undoubtedly, variations in the reactor inlet pressure created differences in the reactant concentrations and hence in the observed reaction kinetics. Moreover, the lower pressures observed at the catalyst inlet may have been indicative of channeling, i.e., short-circuiting or bypass of reactants through or around a portion of the catalyst bed. Therefore, the results of the previous poisoning study must be discounted.

In previous reports, activity data were reported as NO conversions. In this report, we have assumed first-order reaction kinetics (Eq.(1)) and computed first-order rate constants by performing a material balance across the packed bed and integrating the resulting expression (Eq. (2)), as did Chen *et al.* In this way, our results are directly comparable to the literature results. In addition we conducted new experiments with particles more carefully size-classified and more carefully packed in the reactor. We discuss the kinetic expressions first and then the sample preparation.

In our analysis, r_{NO} is the rate of reaction of NO, C_{NO} and $C_{NO,0}$ are local and *inlet* NO concentrations, respectively [moles/volume], k is the rate constant [$cm^3/g/s$], $F_{NO,0}$ is inlet feed rate of NO [moles/time], X_{NO} is NO outlet conversion, and W is weight of catalyst [g]. Eq. (2)

contains variables that are known or measurable and thus the observed first-order rate constant, k_{obs}, may be determined from experiment.

$$-r_{NO} = kC_{NO} \tag{1}$$

$$k_{obs} = \frac{F_{NO,0}}{C_{NO,0}W}\ln(1 - X_{NO}) \tag{2}$$

It should be emphasized that Eq. (2) rests on several assumptions, which are listed below.

1. The gas flow through the bed is uniform with no significant radial or angular flow or concentration gradients.
2. The catalyst bed is isothermal.
3. Expansion effects due to reaction stoichiometry or pressure changes across the bed are negligible.
4. The rate can be modeled according to a first-order model.
5. Film mass transfer and catalyst pore diffusion effects are nonexistent (i.e. the gas composition at any axial position through bed, including inside the pellets, is uniform).

Experience running the reactor system gives us reason to believe that Assumptions 1 and 2 are justified. In the case of Assumption 3, reactant concentrations are so low that expansion due to stoichiometry is negligible. However, pressure does change through the bed. Knowing pressure through the catalyst bed is important because it affects the value of $C_{NO,0}$ in Eq. (2) and consequently the calculated rate constant.

Figure 17 is a conceptual representation of the pressure levels through various parts of the packed reactor tube as gas is passed through it at high catalyst space velocities. In the figure, the labeled points are (a) the catalyst upstream void space, (b) the bottom Pyrex wool plug, (c) the stainless steel catalyst bed support frit, (d) packed catalyst bed, (e) top Pyrex wool plug, (f) and reactor exit. (g) and (h) indicate, respectively, the catalyst plug inlet and outlet pressures; the difference in their values is the catalyst bed pressure drop.

Determination of the pressure at any point inside the catalyst bed is difficult. We have found, however, that running a reactor empty without catalyst (but with the frit and Pyrex wool plugs) gives a very low inlet pressure reading on the pressure transducer as compared to tubes with packed catalyst. Thus, it seems that the greatest source of pressure drop is the catalyst bed, and it would thus appear that the upstream pressure transducer readout is very close to the catalyst bed inlet pressure. We further treat the pressure drop through the catalyst bed as negligible. This means that the model for computing the value of $C_{NO,0}$ in the rate constant calculation assumes that the *entire* catalyst bed pressure is equal to that of point (g) in Figure 17, and the point (g) is approximately equal to the upstream pressure measurement at point (a). Although this assumption is only approximate, it is the best estimate we have at this time and has reduced much of the variation in the observed rate constants as compared to the cases where a steady inlet pressure of 1 atm was assumed.

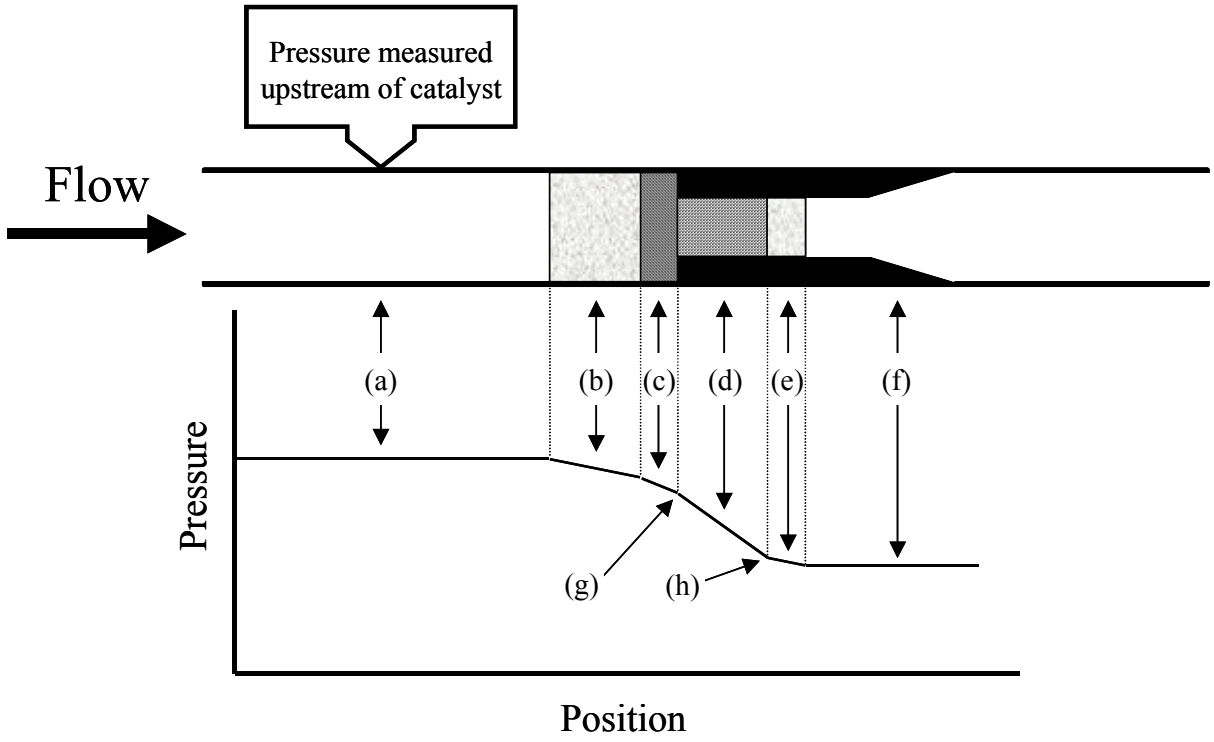

Figure 17. Schematic of pressure drop along packed reactor tube. See text for description of labeled points.

Assumption 4 was that the reaction can be modeled according to a first-order expression, which may not be the case. One empirical power equation for rate of NO decomposition, shown in Eq. (3), is given by Busca, Lietti, *et al.* (1998). α has been reported by some researchers to be 1 on vanadia-based catalysts, while other authors report lower values ranging from 0.5-0.8. It is further stated that "[w]orking in excess of oxygen and in the absence of water vapor or with water contents above 5%, the rate dependencies from oxygen and water can be neglected." Such conditions exist in our reactor and should result in a rate expression in the form of Eq. (4). The dependency of NH_3 concentration can also be neglected if $NH_3/NO \geq 1$, thus reducing to Eq. (1).

$$-r_{NO} = kC_{NO}^{\alpha}C_{NH_3}^{\beta}C_{O_2}^{\gamma}C_{H_2O}^{\delta} \tag{3}$$

$$-r_{NO} = k`C_{NO}^{\alpha}C_{NH_3}^{\beta} \tag{4}$$

However, some authors have reported that when working with sub-stoichiometric ammonia (i.e. $NH_3/NO < 1$, as is often the case in industry where minimal ammonia slip is important), the rate dependence of NH_3 concentration appears with a β near 0.2. Other studies have concluded that since SCR activity correlates with Brønsted-adsorbed ammonia, the mechanism should be Eley-Rideal, where gas-phase NO reacts with adsorbed ammonia. If this is the case, then the rate law might be appropriately modeled by Eq. (5), which may give $\beta \approx 0.2$ if Eq. (4) is used to model the reaction. (See Busca, Lietti, *et al.* for references to all kinetics studies.)

$$-r_{NO} = kC_{NO}\frac{C_{NH_3}}{1+KC_{NH_3}} \qquad (5)$$

Our assumption that Eq. (1) (first order in NO and zero order in NH_3) is a valid rate model may be somewhat approximate at NH_3/NO = 1. However, this assumption was used by Chen, Buzanowski, *et al.* in their calculation of rates and appears to fit our data well. By making the same assumption, we are able to compare our results directly with theirs.

Finally, Assumption 5 is that film mass transfer and pore diffusion effects are unimportant. To test this hypothesis, effects of pore diffusion resistance were tested by running fresh catalyst that was sieved into four different size fractions at temperatures ranging from 250 to 400 °C. During reaction, water vapor (10%) was introduced in a reactant gas stream composed of 900 ppm NO, 900 ppm NH_3, 2% O_2, and balance He. Fifty mg of catalyst was used, and gas flow rate through the catalyst bed was 380 sccm.

Prior to reaction, the catalyst was "steam treated" overnight at around 400 °C with 10% water, 2% O_2, balance He at 150 sccm total flow. The steam treatment was expected to stabilize catalyst activity, as a decrease in conversion with time had been observed in the past. No drift in conversion was apparent when the reaction was run wet, although a slight downward drift in conversion was still seen when the catalyst was run dry, even after the steam treatment.

The observed rate constants for various particle sizes as a function of temperature are shown in Figure 18. Consistent with theory, particle size has a significant effect on the observed rate constant presumably because of pore diffusion resistance, and the observed drop in activity with increasing temperature becomes more important with increasing particle size.

At the smallest and larges particle sizes, these data agree very well with expected behavior. One observation we have not yet been able to explain is that the data from the 147-180 μm and 212-250 μm fractions overlap. One possible explanation is that the average particle size is close to the upper and lower limits of particle size for the smaller and larger fractions, respectively. We also assume that catalyst activity is uniform with position and particle size; non-uniformities may also explain differences in rate constants for different particle sizes.

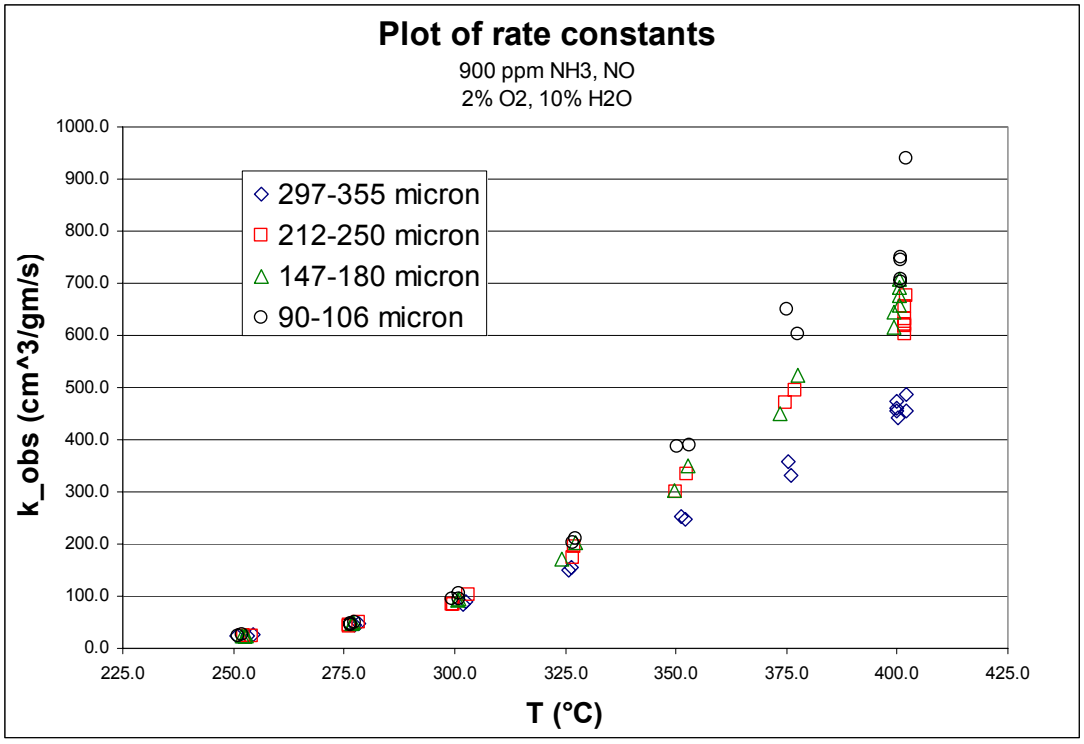

Figure 18. Observed rate constants versus temperature for four sizes of catalyst pellets.

Figure 19, an Arrhenius plot of the data, shows a trend of greater non-linearity as particle size increases. Figure 20 is an expanded Arrhenius plot of the same data from this study that also includes data from Chen, Buzanowski, *et al.* In analyzing their data, we used physical constants from our catalyst where we did not have such data for their catalyst. These include pore size, porosity, and Thiele modulus. The curvature of their data suggests that strong pore-diffusion resistance greatly affected their results at higher temperatures. Chen et al. concluded that poisoning decreases catalyst activity monotonically. This conclusion would not change based on our analysis. However, the intrinsic rate constants associated with their results do depend on the extent of pore diffusion and pore diffusion complicates the estimation of this rate constant. It is in these quantitative details that the effect of particle size makes the most difference.

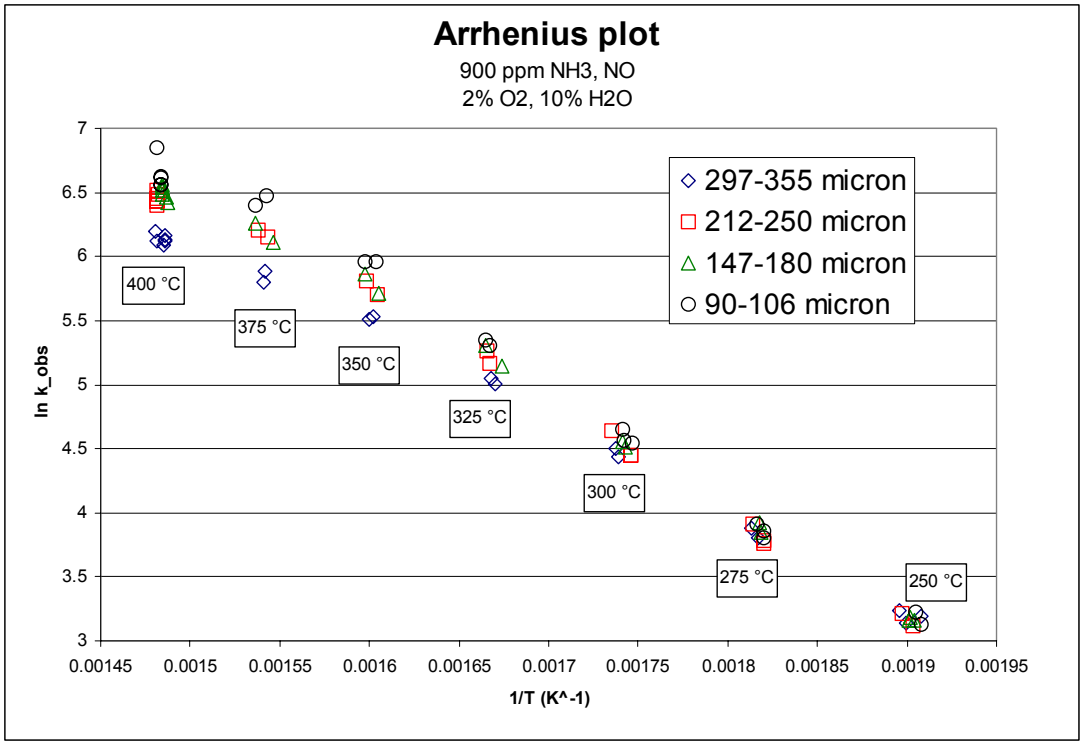

Figure 19. Arrhenius plot of our data.

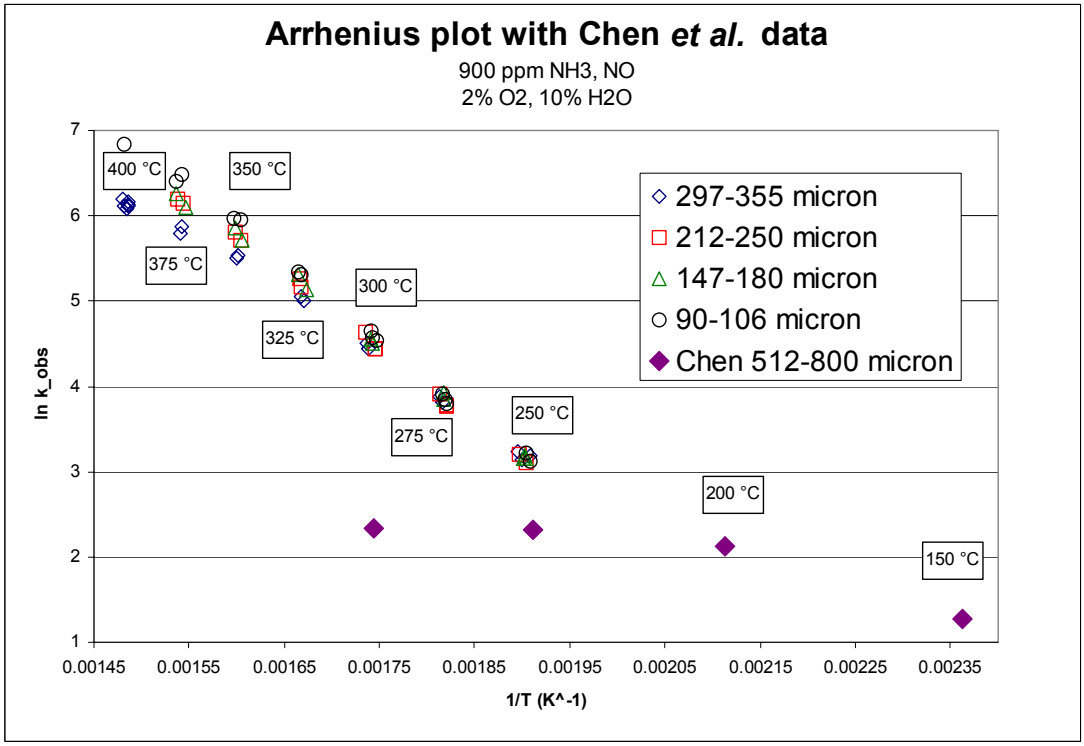

Figure 20. Arrhenius-type plot of our data and other published data (Chen, Buzanowski *et al.* 1990).

The effects of pore diffusion resistance on concentration profiles in pores and on reaction rate were estimated by calculating Thiele modulus and effectiveness factors for spherical pellets.

First, average pore size and total void fraction were obtained by running samples of fresh catalyst in a Micromeritics™ TriStar 3000 instrument. The average void fraction was around 55%, giving a particle density, ρ_{pellet}, of about 2.3 gm/cm^3. Average pore diameter was found to be 53 nm. The average pore diameter was used along with diffusivity correlations to estimate the effective diffusivity, D_{eff}, of NO inside the pores of the pellets as a function of temperature and pressure. Average pellet diameter, d_{pellet}, was assumed to be the median of high and low values of the particle fraction size. ρ_{pellet}, and D_{eff} were used in Eq. (6) to compute the Thiele modulus, ϕ.

$$\phi = \frac{d_{pellet}}{6}\sqrt{\frac{k_{int}\cdot\rho_{pellet}}{D_{eff}}} \qquad (6)$$

Also appearing in Eq. (6) is the intrinsic rate constant, k_{int}. This was obtained by fitting the data obtained on the smallest particles, the 90-106 micron fraction, to an Arrhenius model for the rate constant (Eq. (7)). The fit was performed by least squares method in Excel on all the data up to and including 375 °C (data inside dashed oval in Figure 21). Data obtained at the highest temperature, 400 °C, were excluded because they were quite scattered and did not appear to fall on the smooth curved line corresponding to the best fit of the data. The activation energy, E_a, and pre-exponential factor, k_0, were 72.9 kJ/mol (17.4 kcal/mol) and $4.57\cdot10^8$ cm^3/gm/s, respectively. These values were used to calculate values of k_{int}, which could then be used in Eq. (6) to find the Thiele modulus.

$$k_{int} = k_0 \exp\left(\frac{-E_a}{RT}\right) \qquad (7)$$

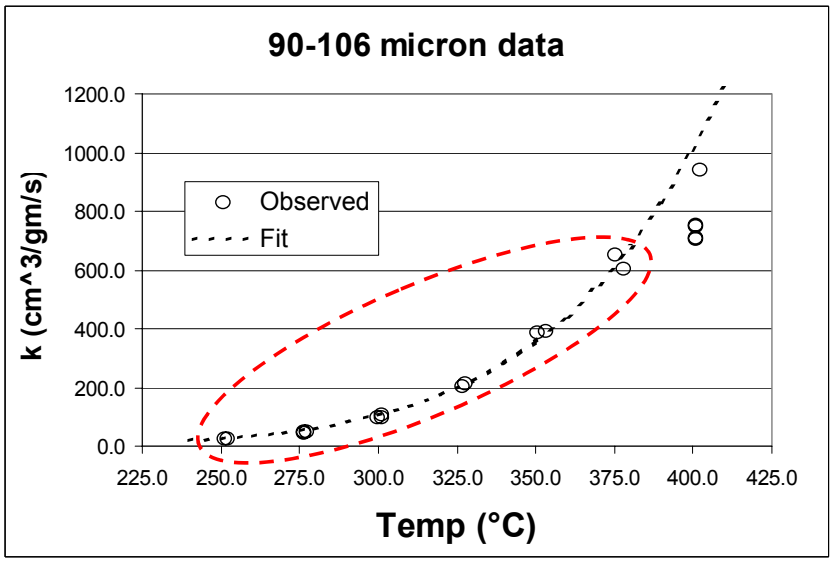

Figure 21. Plot showing points from which kinetics parameters were fit.

The effectiveness factor, η, was computed according to Eq. (8), a correlation for spherical particles. (Another assumption made here is that the particles in our tests were spherical). The intrinsic rate constant expression, Eq. (7), was then multiplied by this effectiveness factor to

obtain a predicted rate constant, k_{pred}, as a function of temperature and particle size as in Eq. (9). The predicted rate constants are plotted as lines along with the observed data points in Figure 22.

$$\eta = \frac{1}{\phi}\left(\frac{1}{\tanh(3\phi)} - \frac{1}{3\phi}\right) \tag{8}$$

$$k_{pred} = \eta \cdot k_{int} \tag{9}$$

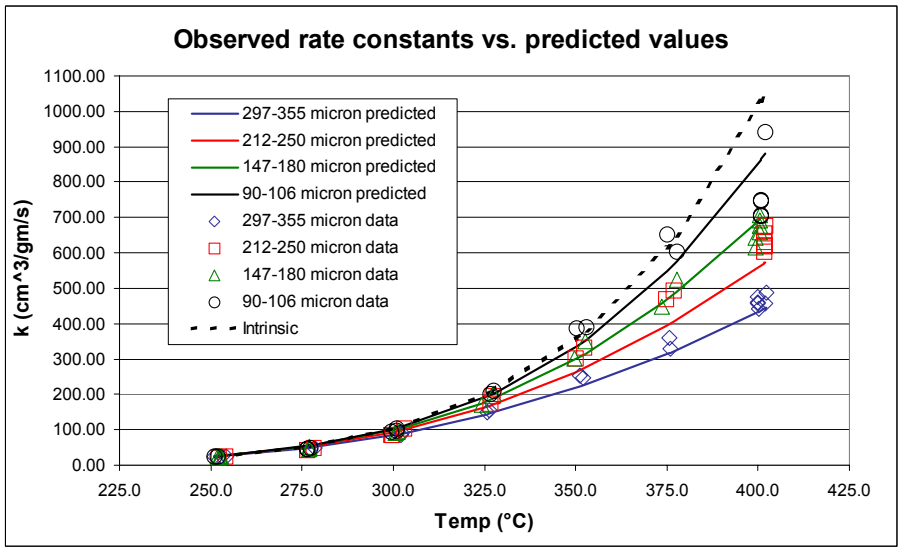

Figure 22. Plot of observed data vs. predicted values for various particle sizes.

It is evident from Figure 22 that rate constants predicted by Eq. (9) fall very close to observed rate constants computed from Eq. (2). It is important to mention that it was *assumed* that the 90-106 μm particle sizes operate in the intrinsic regime up to 375 °C in order to obtain values for E_a and k_0 used in predicting the Thiele modulus. Figure 22 illustrates, however, that the *predicted* rate constant values for the 90-106 μm fraction (topmost solid line) are *below* the assumed intrinsic data (dotted line). This means that the E_a and k_0 values are not intrinsic, but should nevertheless be very close to the true values. Fortunately, the effects of pore diffusion resistance do not really manifest themselves to an appreciable extent until the reactor temperature reaches around 375 °C.

Estimates of gas-phase mass transfer coefficients indicate that film mass transfer resistance is at most a few percent of the total resistance to reaction. Thus, film mass transfer resistance is not appreciable under the conditions of this study and was therefore neglected.

In view of these results, we feel comfortable running tests with powders in the 90-106 micron range since they do not appear to be significantly affected by mass transfer or pore diffusion limitations until the reactor temperature exceeds 375 °C, at which point the effectiveness factor drops below 0.9 (see Figure 23).

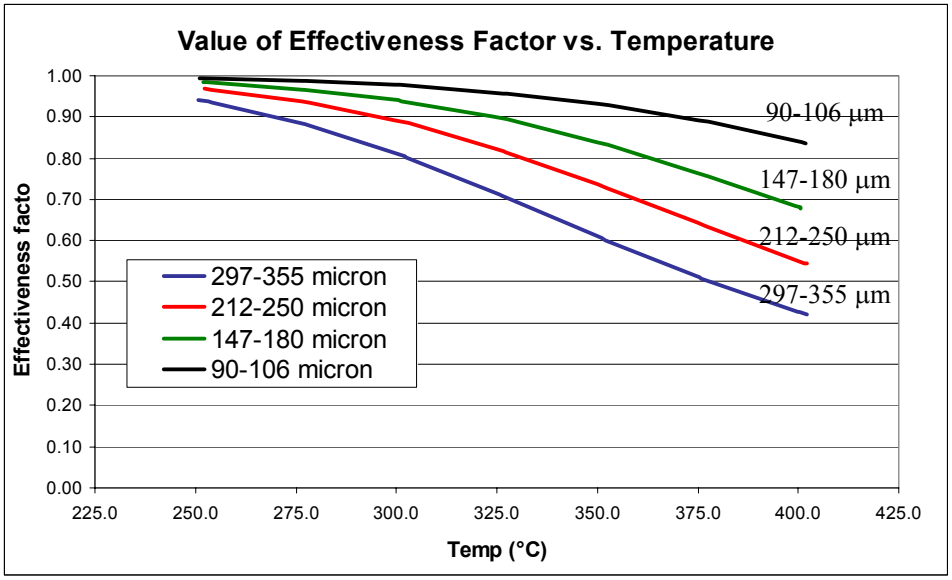

Figure 23. Plot of effectiveness factor, η, versus temperature for various pellet sizes.

Poisoning study

A poisoning study similar to that reported by Chen, Buzanowski, *et al.* was conducted on the BYU SCR catalyst in the 90-106 micron particle range that had been poisoned at various levels with Ca and Na by a previous student. In our study, 50 mg of catalyst was used. Prior to reaction, the catalyst was "steam treated" overnight at around 400 °C with 10% water, 2% O_2, and balance He at 150 sccm flow (as described above). The reaction conditions of the two studies are compared in Table 2.

Data obtained from running the catalyst both wet and dry are shown in Figure 24. In this figure, it can be seen that addition of water vapor appears to inhibit the reaction (i.e. reduces the value of the observed first order rate constant), while it can also be seen that Na is a stronger poison than Ca, resulting in almost complete deactivation when the Na:V ratio is 1. Ca is not as strong of a poison at the same poison-to-vanadium atom ratio. This is consistent with the fact that Na is more strongly basic and thus has a greater effect on the surface Brønsted acidity.

Table 2. Comparison of conditions in poisoning study by BYU to those of Chen, Buzanowski, *et al.*

	BYU	**Chen, Buzanowski, *et al.***
Catalyst Composition	1% V_2O_5-9% WO_3/TiO_2	5% V_2O_5/TiO_2
Poisons	Ca, Na	Ca, Na, K, Li, P, As, Pb, Rb, Cs
Reaction Conditions	340 °C NO = NH_3 = 900 ppm 2% O_2 10% H_2O (when used) balance He flowrate = 380 sccm (estimated ~1,000,000 hr^{-1} based on solid catalyst volume with 0.022 cm^3-50 mg-catalyst)	300 °C NO = NH_3 = 1000 ppm 2% O_2 no H_2O balance N_2 space velocity = 15,000 hr^{-1} (500 sccm with 2 cm^3 of pellets)
Pellet/granule sizes	90-106 μm (170-140 mesh)	500-812 μm (32-20 mesh)
BET surface area	~32 m^2/g	30.6 m^2/g

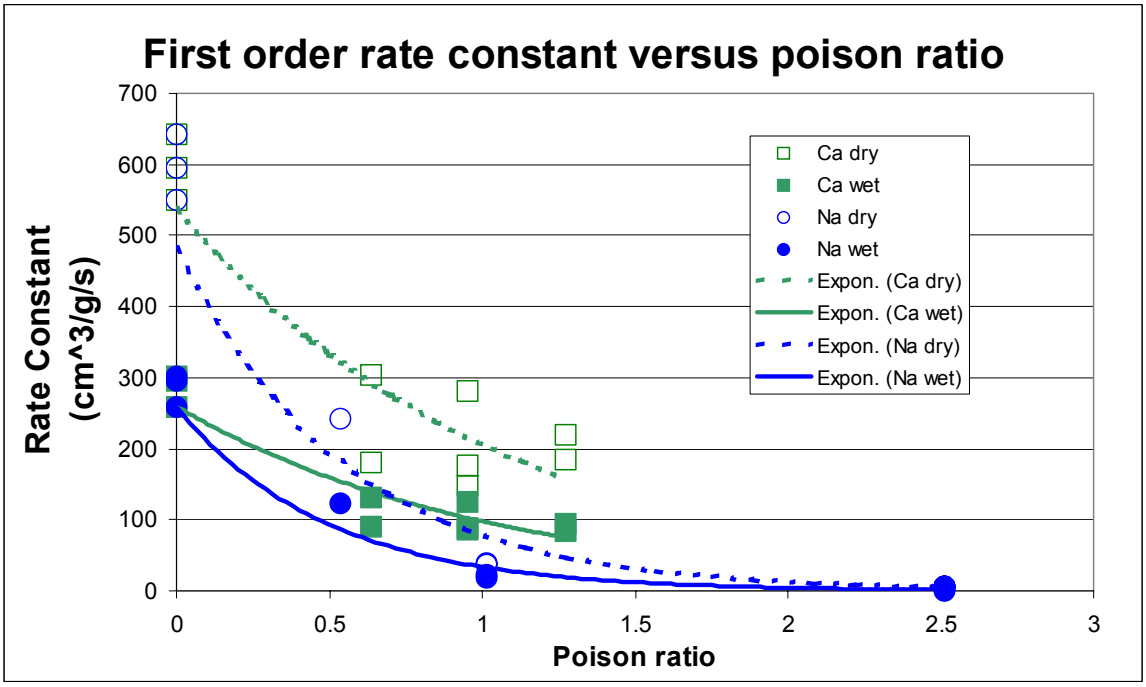

Figure 24. Plot of observed rate constants at various poison levels for Na, Ca with and without water.

Normalized catalytic *activity* as a function of poison level is shown for Ca (Figure 25) and for Na (Figure 26). Normalized activity is defined here as the observed rate constant at any given poison level divided by the observed rate constant for the fresh catalyst. Data obtained on the same poisons by Chen, Buzanowski, *et al.* are also plotted in these figures for easy comparison.

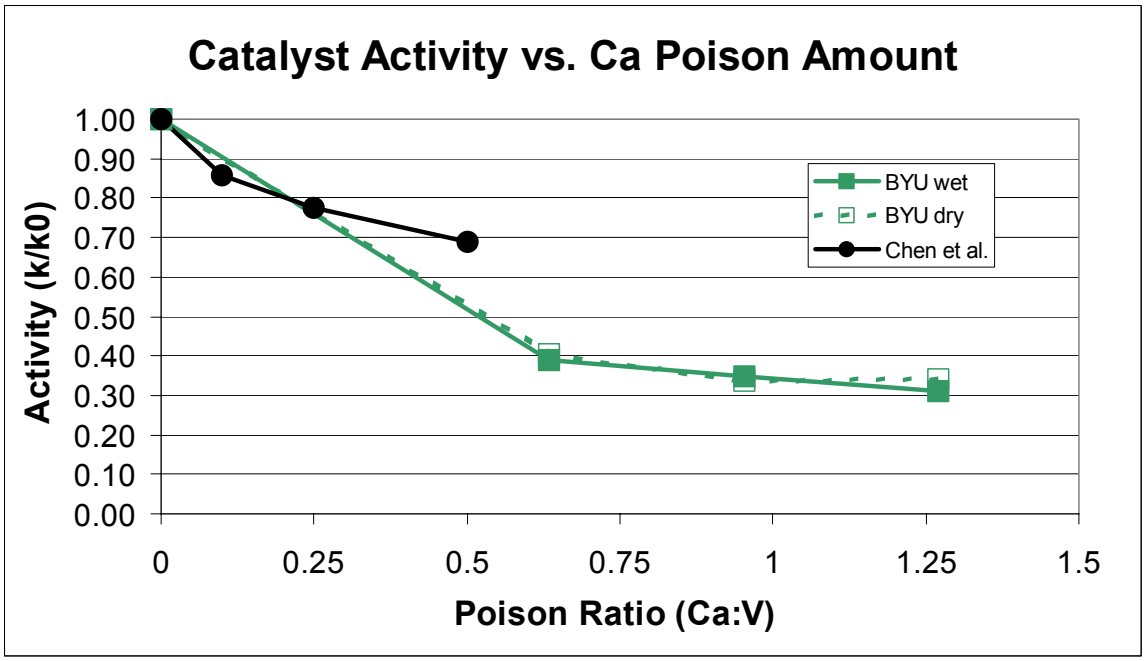

Figure 25. Catalyst activity versus Ca:V ratio.

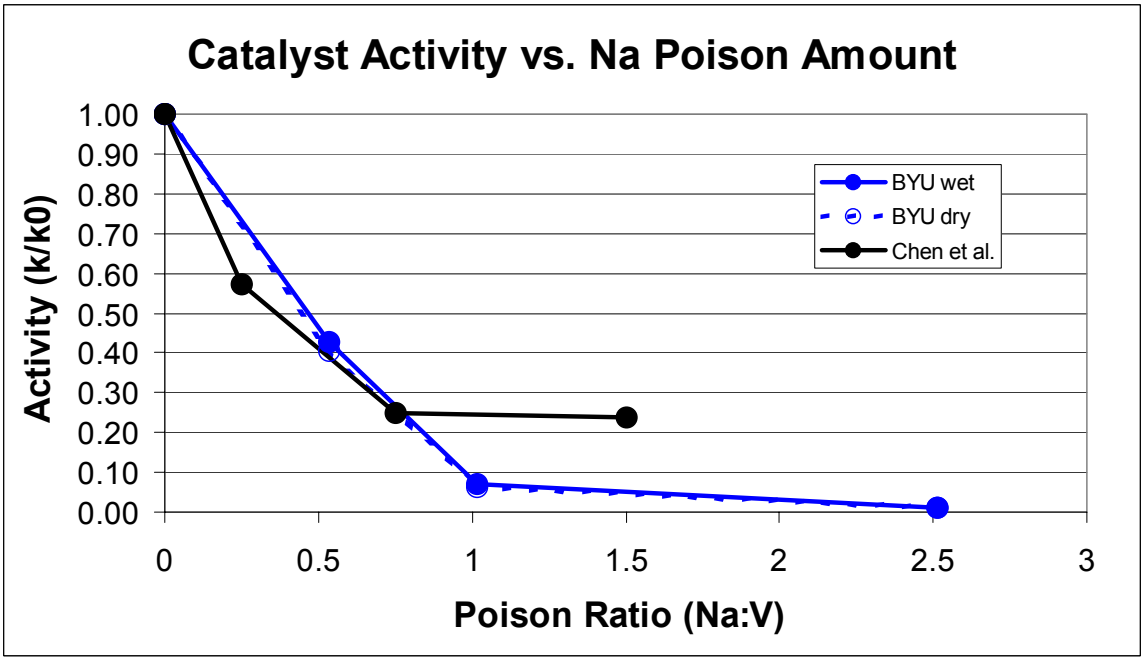

Figure 26. Catalyst activity versus Ca:V ratio.

Two observations are important at this point. First, although addition of water vapor does lower the observed rate constant, it does not affect normalized activity. Second, the same trends in

activity loss with poison ratio are observed in the two studies for both poisons, i.e., the activity levels off at a higher value for Ca-doped catalysts relative to Na-doped catalysts. The Na-doped catalysts of this study were essentially completely poisoned at Na:V = 1, in contrast to the Ca-poisoned samples, which appeared to level off at around 30% of original activity. Activity results from higher Ca:V ratios would reveal whether activity truly levels off.

Commercial monolith work

Monolith test reactor shakedown

The monolith test reactor (MTR) was completed and operated for a short time during this quarter and has been used in preliminary studies on one commercial catalyst (M11). The completed reactor is shown in Figure 27.

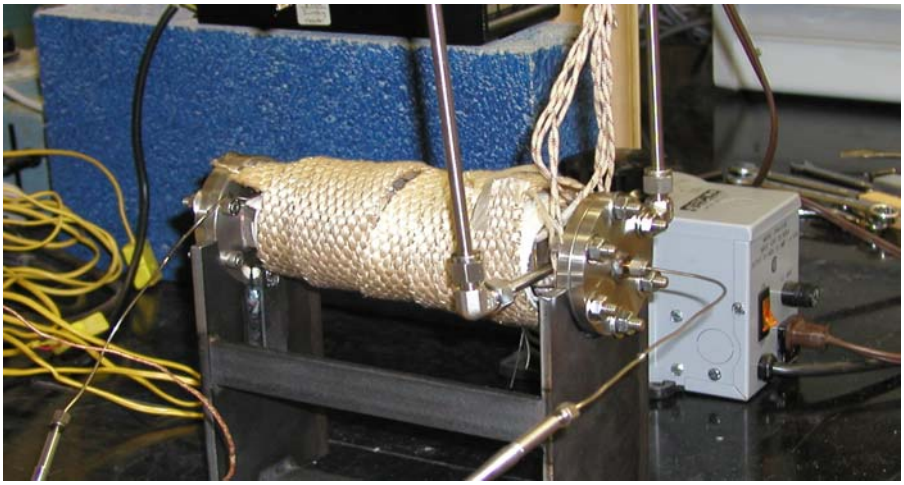

Figure 27. Photo of finished MTR as it appears when operating.

Monolith catalysts are prepared and charged to the reactor as follows. A monolith sample is prepared by carefully cutting it with a scroll saw, after which it is wrapped in ceramic felt or wool and slid snugly inside an aluminum sample holder, which is inserted inside the MTR and kept in place by an internal spring. In the case of a plate catalyst, samples may be inserted into slots that run along sample holder. Figure 28 shows the two types of catalyst sample holders.

1 Note that this corresponds to catalyst C6 in the slipstream reactor.

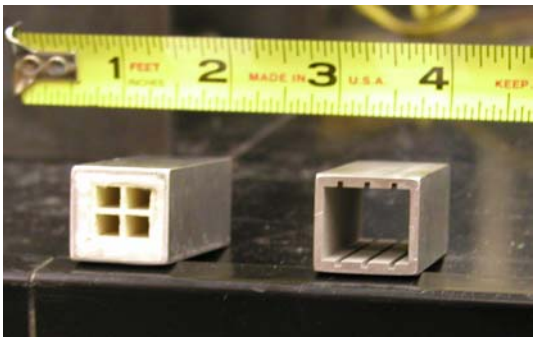

Figure 28. Photo showing monolith piece inside sample holder (left) and empty slotted plate catalyst sample holder (right).

After insertion of the sample holder, the end flange of the MTR is attached and inert gas flow is introduced as the whole device is heated by four external plate heaters. Temperature is controlled manually by an external variable AC transformer and measured by two thermocouples—one extending inside the MTR chamber just downstream of the catalyst exit and the other fastened to the outside of the MTR body between two of the heater plates on one of the corners.

First, a blank run was conducted with a (presumed) non-catalyzed cordierite monolith inserted in lieu of the vanadia-based SCR catalyst. NH_3 (900 ppm), NO (900 ppm), O_2 (2%), and He (balance) were flowed through this blank reactor as temperature was slowly raised to 400 °C.

At constant gas inlet composition, the outlet NH_3 concentration began to diminish at around 310 °C, while the outlet NO concentration increased. The extent of these changes increased with increasing temperature. NO reached a maximum of around 1015 ppm at 400 °C, while NH_3 reached a minimum of around 600 ppm at that temperature. Thus, it appears that NH_3 is oxidized to NO (and perhaps NO_2) over the uncatalyzed monolith, although the NO_2 and total NO_x signals *decreased* along with the increasing NO signal, indicating that NO_2 was probably not being formed.2

A short explanation of the operation of our NO_x analyzer might be helpful. This instrument can only measure NO concentration directly. To obtain a total NO_x reading (and thus NO_2 by difference), it converts any NO_2 present in the sample stream to NO by passing the sample gas through a stainless steel chamber heated anywhere from 550 to 800 °C (nominal is 650 °C). Similarly, at higher temperatures it is possible that our MTR converts NO_2 to NO if NO_2 is present in the gas feed. More likely than not, these observations may explain the decreasing NO_2/total NO_x signals as measured by our NO_x analyzer.

Two possible explanations for NH_3 oxidation are hypothesized. First, the oxidation reaction may occur on the stainless steel (SS) surfaces of the reactor, although we have not seen similar effects in our powdered catalyst reactors, which have been run blank (without catalyst) at temperatures up to 400 °C. However, where 316 SS was used in the construction of our powdered reactors, the MTR is composed of 304 SS since this was the only material available for square tubes. It is possible that the observed oxidation occurs on 304 SS but not on 316 SS surfaces, although

2 Although this instrument has only been calibrated for NO, not NO_2, and may thus give confusing information on the NO_2 and total NO_x channels.

oxidation of ammonia on the reactor walls is unlikely in view of their low surface areas. Second, it is possible that the cordierite catalyzed the ammonia oxidation reaction.

Conversion data from commercial monolith M1

At the time the NH_3 oxidation was observed, we chose to measure conversions on actual catalyst samples at a "safe" temperature of 300 °C rather than troubleshoot the oxidation issue described above. Three runs on commercial M1 were performed, two on fresh samples, and one on an exposed sample (~2000 hours exposure time). Feed composition was 900 ppm NO, 900 ppm NH_3, 2% O_2, and balance He (no H_2O in this test). The channel width of M1 was 6.2 mm and the wall thickness was 1.2 mm. This translates into a total catalyst void volume (volume available to gas flow) of 4.77 cm^3 and a total catalyst block volume of 6.79 cm^3.
Results are shown in Figure 293 as NO and NH_3 conversion plotted against space velocity, which was based on overall catalyst block volume at a standardized gas temperature of 0 °C. The catalyst pieces were each 31 mm long and consisted of four channels. The exposed monolith piece tested in the MTR was cut from the front of M1 in a somewhat aggressive manner with a scroll saw. During this process, much of the fouling deposit on this section of the catalyst was dislodged. The remaining loose, fouling deposit on the catalyst surface was cleaned off by blowing with compressed air, although some small deposits remained. The intention was that any differences in observed catalyst performance of fresh and exposed samples would be attributable to deactivation by poisoning (and perhaps only slightly to pore plugging) rather than by masking. As will be shown later, even these cleaned catalyst surfaces were substantially contaminated with ash deposits.

3 In this figure, NH_3 concentration may have been in excess of 900 ppm (resulting in $NH_3/NO > 1$) as NH_3 conversion was consistently below NO conversion. We are currently examining discrepancies in analyzer calibration gas and process gas concentrations.

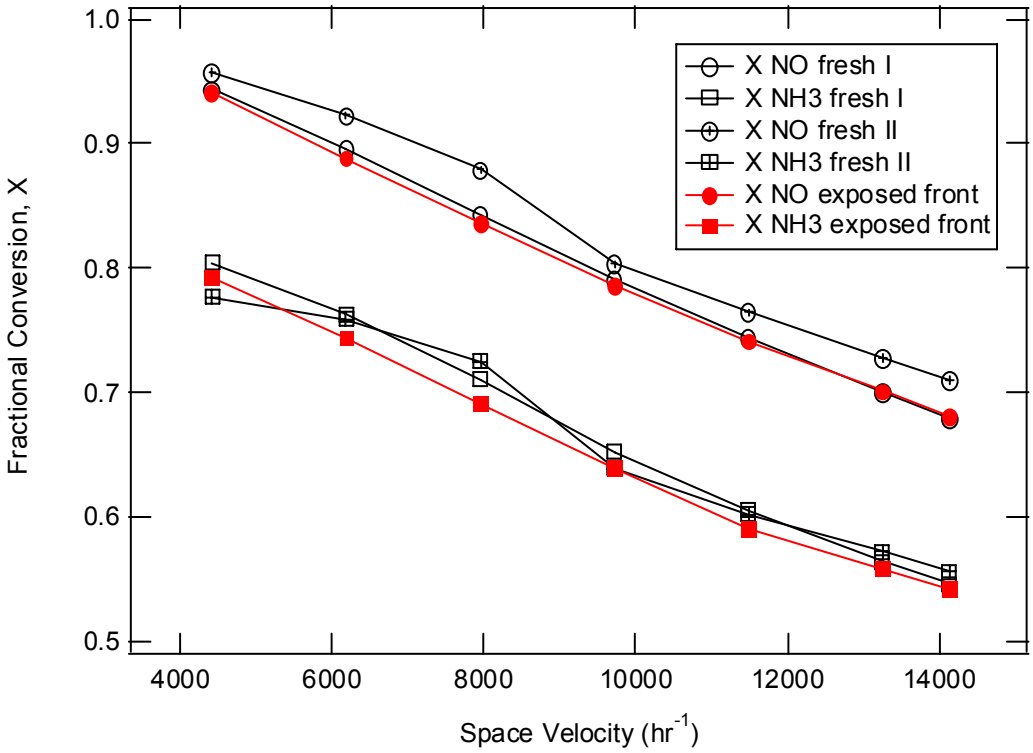

Figure 29. Fractional conversion of NO, NH_3 versus space velocity for one exposed and two fresh M1 samples.

It should be noted that as flow rate increases through the MTR, pressure increases because all exit gas passes through sintered metal filters located between the MTR and the gas analyzer equipment. The effects of flow rate on pressure were consistent between all three runs, as shown in Figure 30. The increase in pressure has two effects on observed catalyst performance. First, it results in increased concentration of reactant species through the catalyst. Second, it results in increased overall gas density, and therefore decreased flow rate/linear velocity through the catalyst (i.e. longer residence time) as would be predicted by calculating these values from the inlet gas flow rate in sccm (*standard* cm^3/min) using temperature as the only conversion factor. Thus, if the *actual* space velocity or flow rate based on reactor conditions is desired (again, here the *standard* space velocity is reported for gas flow at 0°C and 1 atm pressure), both temperature and pressure need to be considered in such conversions. This pressure effect is important to consider if any quantitative kinetics data are desired.

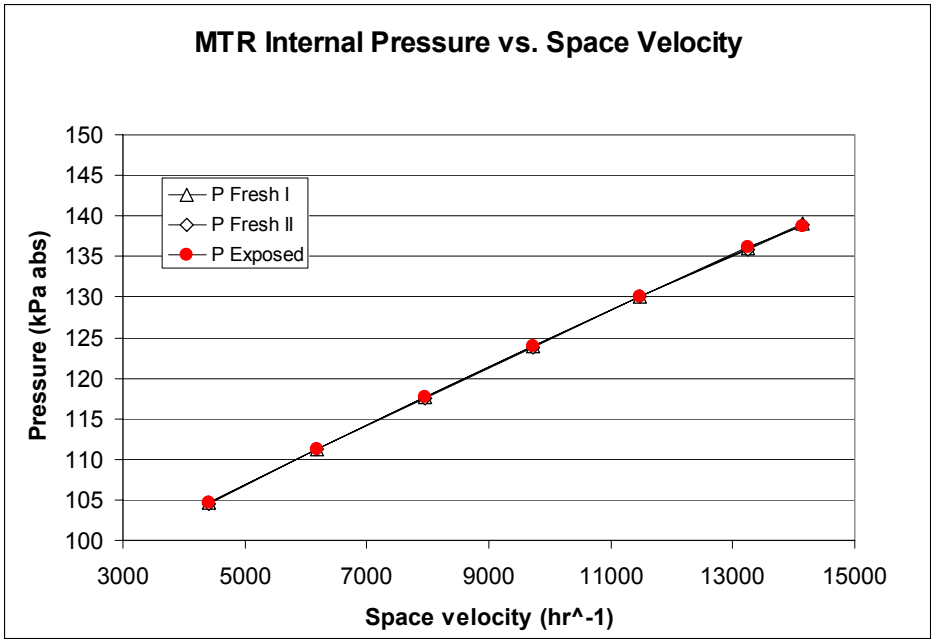

Figure 30. Reactor pressure in kPa abs for three M1 test runs.

Other than gas space velocity, temperature had the greatest effect on NO and NH_3 conversion. As can be seen in Figure 31, the average reactor temperatures for the first fresh (T Fresh I) and exposed (T Exposed) runs were fairly consistent and close to one another. However, the temperature for the second fresh run (T Fresh II) fluctuated considerably. The fourth data point at a space velocity around 10,000 h^{-1} excepted, temperature for the second fresh run was consistently higher than the temperature of the other two runs, and so was NO conversion (compare Figure 29 to Figure 31). Careful control of temperature is crucial for making meaningful comparisons between catalysts.

The observed inconsistencies in temperature result from our use of a variable AC transformer (*variac*) to heat the reactor. The variac consists of a dial on the top and an outlet into which the heaters are plugged. The dial must be turned manually to set the reactor temperature. Reproducing the exact position (and thus output voltage) of the dial is not likely between runs. Even if it were, we have noticed that other factors affect reactor temperature. It can be seen in Figure 31 that increasing the flow rate increases the temperature to a point, presumable due to increased convection of heat inside the reactor. Changes in room temperature also influence MTR temperature: on one occasion, the door to the lab was left open to cool the room. As the room temperature dropped by about 3 °C, the MTR temperature dropped by about 3 °C also.

Finally, to heat the reactor rapidly, the variac can be set slightly higher than it would be at the set point that corresponds to the desired steady-state temperature. This method gives the reactor more power initially and can easily result in a temperature overshoot. This appears to be what happened during the Fresh II run, with the variac output being reduced between the third and fourth data points of that run.

Despite these disadvantages, a variac is a good choice as a power source for several important reasons. First, it was cheap (free) and immediately available. Second, it outputs an intermediate voltage variable anywhere from zero to 120 VAC, where other temperature controllers are usually either "on" (120 VAC) or "off" (0 VAC). According to the manufacturer, if the full voltage of 120 VAC were applied to the mica strip heaters, they would burn out almost immediately. Future experiments will be performed with greater attention to temperature control (e.g. greater patience in fine-tuning temperature). In addition, data taken at different temperatures will allow for interpolation between data points. Conversion vs. temperature curves (at constant flowrate) will be useful. Better insulation of the reactor will also be considered.

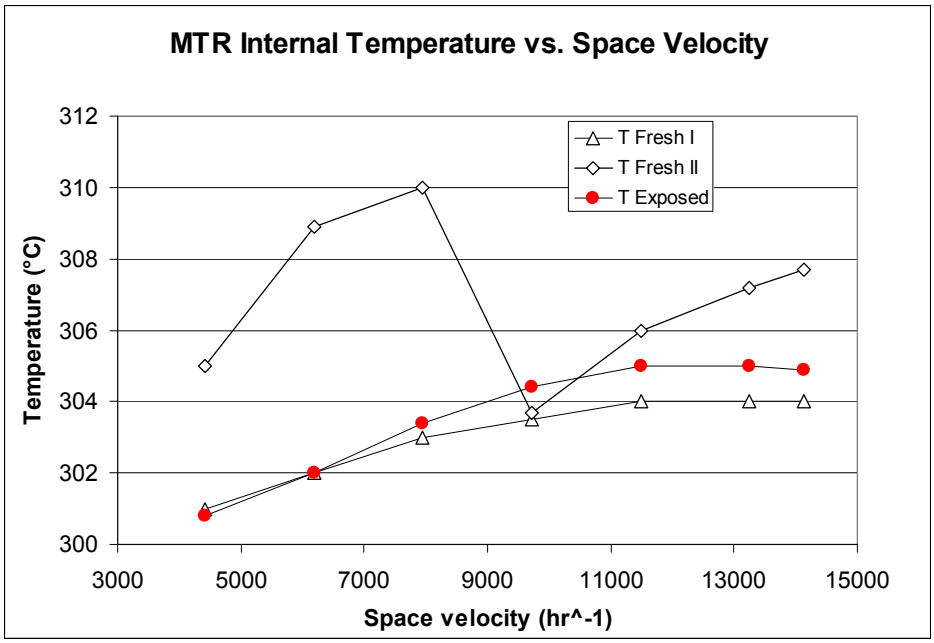

Figure 31. Nominal internal reactor temperature for three M1 test runs.

Two runs with fresh M1 were conducted because in the first fresh run the monolith piece was wrapped in a ceramic felt that contained organic binder (starch), which burned out during the reaction and left black soot-like deposits along some of the catalyst surface. In the other two runs, a different ceramic material that did not "burn out" was used. The resultant fine layer of soot on the first fresh catalyst may partially explain the reduced catalyst activity when the Fresh I and Fresh II NO conversion curves are compared (Figure 29); however, as explained above, it seems more likely that temperature difference is the principal cause of the differences in observed NO conversion.

Results of XPS analysis on M1

XPS tests were run on fresh and exposed pieces of M1. Figure 32 shows a survey scan on the fresh catalyst surface. Peaks corresponding to important elements are labeled. Although the expected location of the vanadium peak is indicated, no peak was noticed in this region, likely because the vanadium content is below detectible levels of the instrument (about 1%). It is also

possible that the V-peak is masked by the very strong O-peak. However, the other metals on the surface (Ti and W) are evident in the data.

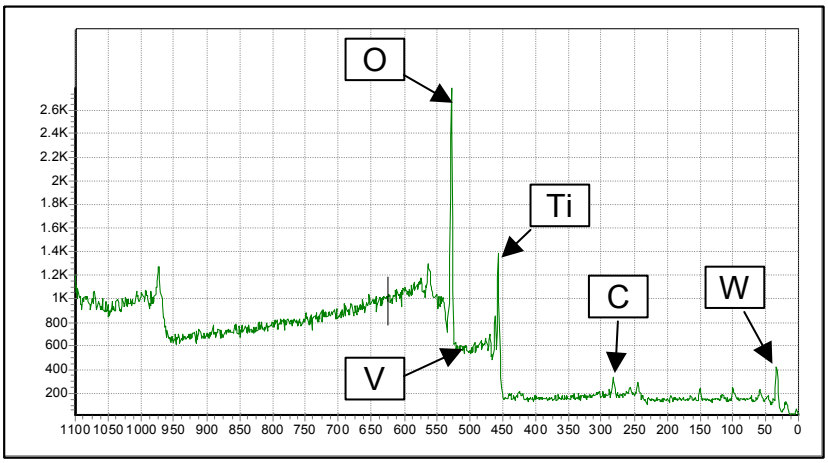

Figure 32. Survey scan of fresh M1.

Figure 33 and Figure 34 are the survey scans for the front and rear (18.5 inches from the front) of the exposed M1 monolith, respectively. In these figures, peaks that do not appear in Figure 32 are identified. These Na, Ca, and S species are attributed to fly ash deposits, much of which had been cleaned off the catalyst surface by blowing through the channels with compressed air. The substantial decrease in the Ti peak and the essentially completely absent W peak suggest that the surface contains substantial amounts of deposited material despite the removal of the deposits during sample preparation.

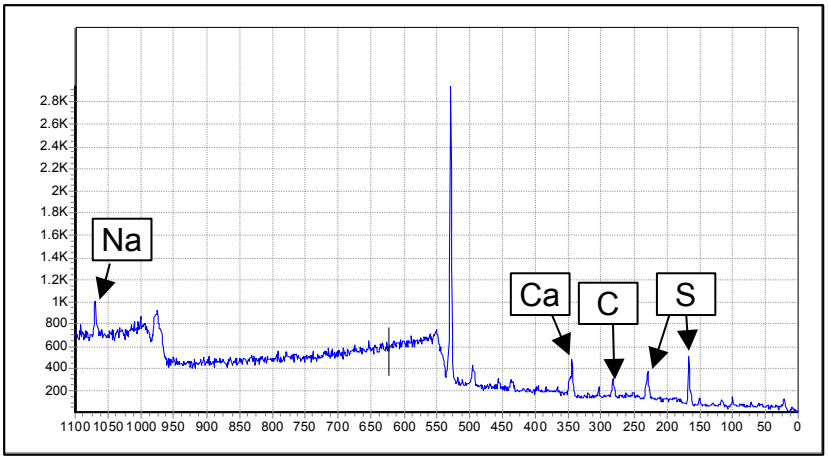

Figure 33. Survey scan of the front of exposed M1.

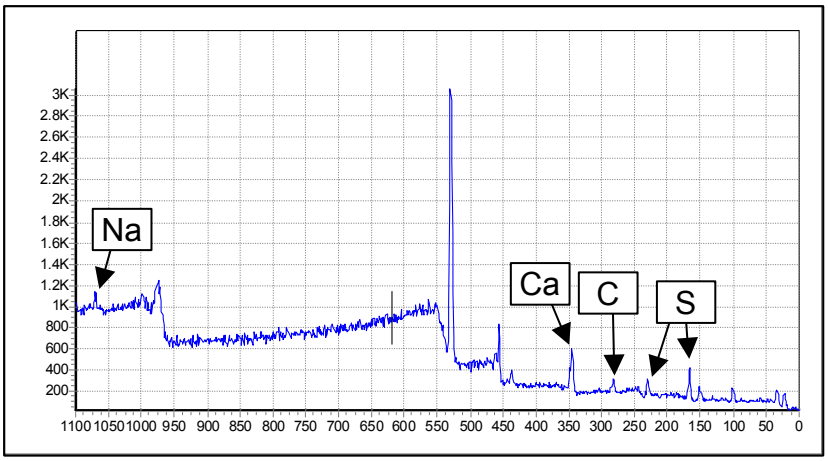

Figure 34. Survey scan of the rear (~18.5 inches from front) of exposed M1.

Task 4.2 Evaluation of Commercial SCR Catalysts for Power Plant Conditions

Catalyst Activity from the Slipstream Reactor

In the last quarter, the slipstream reactor was brought back online after a major outage at the plant. During this quarter, a significant amount of hours for which the catalysts were exposed to the flue gas were accumulated. Figure 35 shows the steady build up of reactor operating time accrued in which the catalysts have been exposed to flue gas for over 1140 hours. Since the start of testing the catalysts have been exposed to a cumulative number of test hours reaching 3800 hours. The slipstream SCR reactor is still running at Rockport. Plans are underway to move the reactor to Gadsden, Alabama in the next quarter.

In this quarter, problems with the Field Point embedded controller have made it difficult to obtain NO_x reduction data continuously from the slipstream reactor. However, it was still possible to obtain NO_x data at specified times. NO_x data were obtained in mid-February and early March. The February 2004 data has been compared with the March/April 2003 and the August 2003 data. It may be recalled that catalyst activity is defined as $\frac{NO_{X(IN)} - NO_{X(OUT)}}{NO_{X(IN)}}$, and is shown in the graphs as NO_x reduction. Figures 36 through 40 show the NO_x reduction data as a function of space velocity for catalysts C2 to C6. All the data shown are for excess ammonia, relative to NO. The NO_x reduction data have, in some cases, been corrected for temperature.

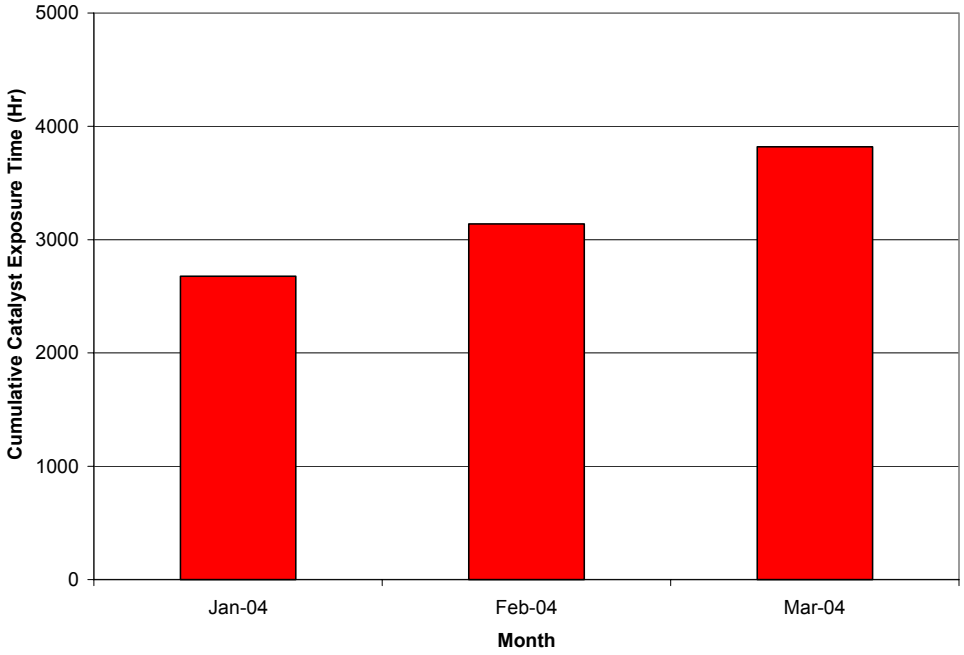

Figure 35. Cumulative catalyst exposure time during the January – March 2004 quarter.

As discussed in the quarterly report for October through December 2003, the August 2003 data were corrected for temperature because the temperature was lower in August than in March 2003 or February 2004. Linear fits of NO_x reduction as a function of temperature over certain ranges of space velocity were used to make the corrections to the August 2003 data (as discussed in the previous quarterly report) and February 2004 data. Thus, the ranges for those data shown on the graphs represent the range of temperatures observed in the March 2003 data; the August 2003 data and the February 2004 data have been corrected to this temperature range using the previously determined temperature coefficients for the individual catalysts.

These preliminary results reveal that there has been a decline in catalyst activity for catalysts C2, C4 and C6. Catalysts C3 and C5 do not appear to have had significant loss in activity. It may also be noted that in April 2003, the catalysts were exposed to flue gas for approximately 750 hours of operating time and by early March 2004, the catalysts had seen well over 3000 hours of operating time in flue gas. Also, the reactor was off-line for twelve weeks, from September through December of 2003, because of a major outage at the plant to install low-NO^x burners. For an overall comparison, all the data discussed above are presented in a general plot as shown in Figure 41. This graph shows the general trend in NO_x reduction as a function of space velocity.

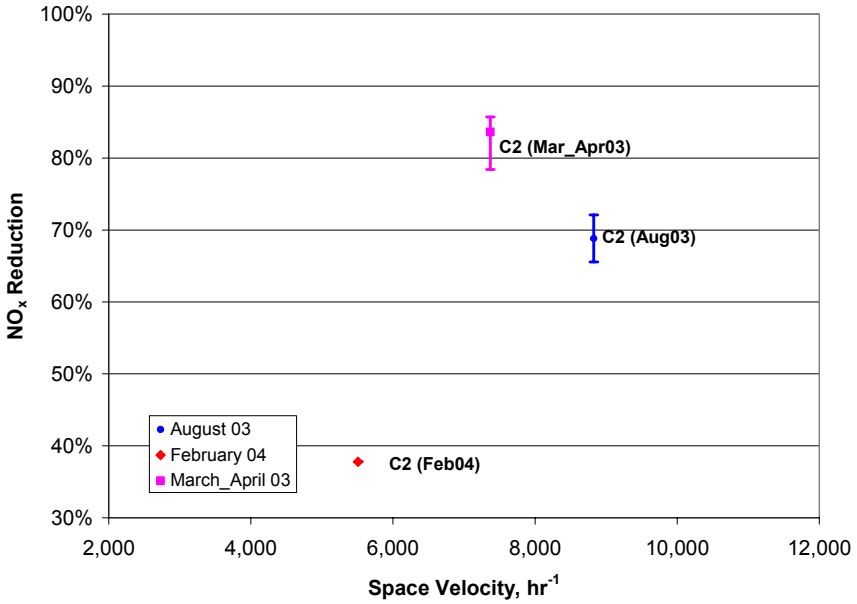

Figure 36. Catalyst activity shown as NO_x reduction as a function of space velocity for catalyst C2. C2 has been corrected for temperature. Temperature range: 653 – 677 °F; NH_3/NO range: 1.0 – 1.29.

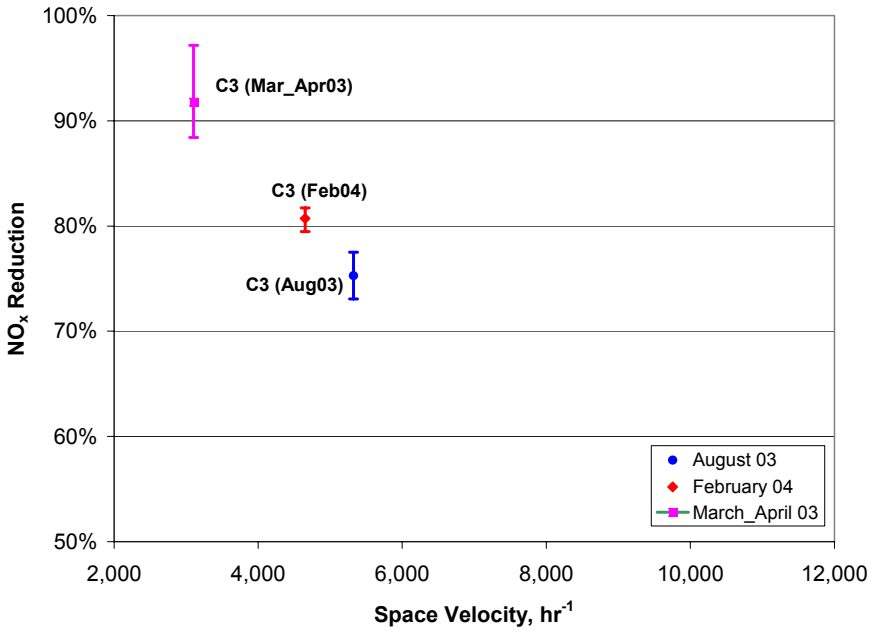

Figure 37. Catalyst activity shown as NO_x reduction as a function of space velocity for catalyst C3. Temperature range: 674-683°F; NH_3/NO range: 0.95 – 1.02.

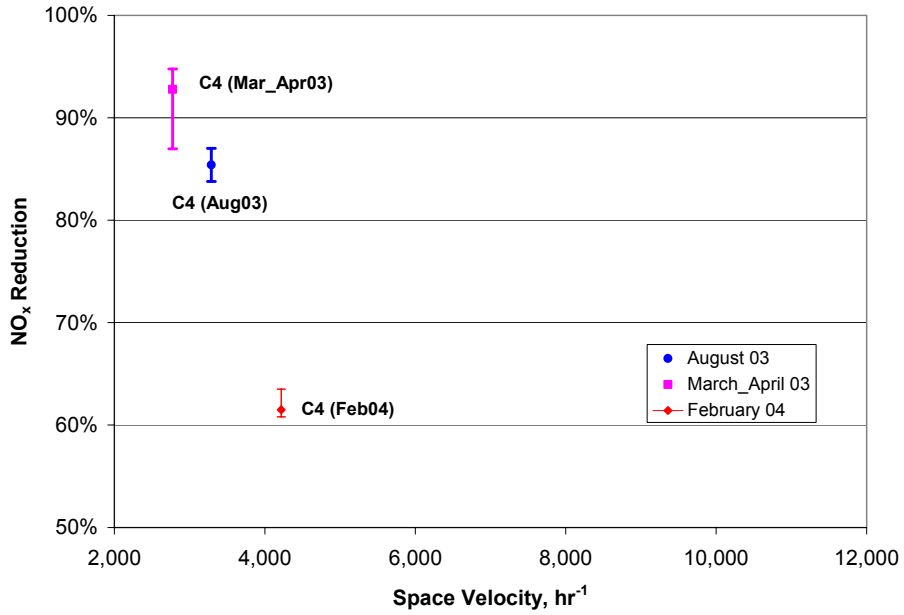

Figure 38. Catalyst activity shown as NO_x reduction as a function of space velocity for catalyst C4. Temperature range: 676-685°F; NH_3/NO range: 0.97 – 1.0.

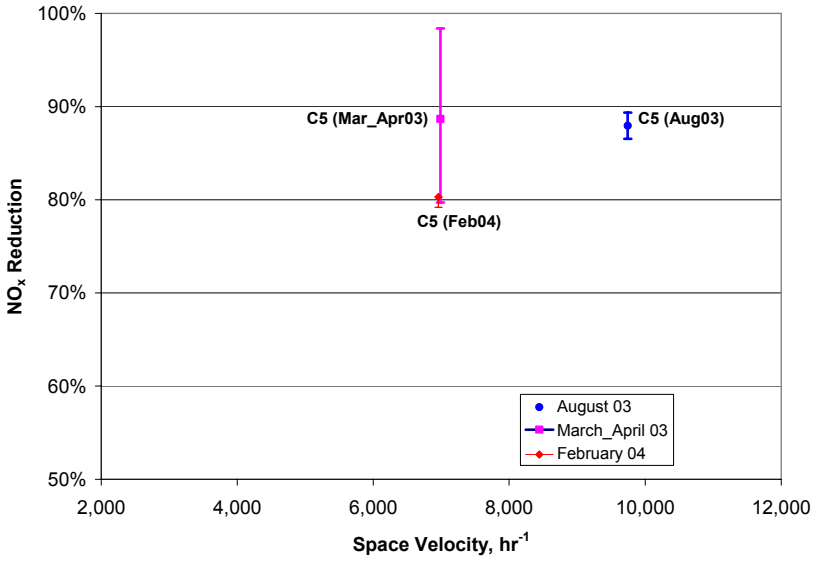

Figure 39. Catalyst activity shown as NO_x reduction as a function of space velocity for catalyst C5. Temperature range: 660-669°F; NH_3/NO range: 0.96 – 1.02.

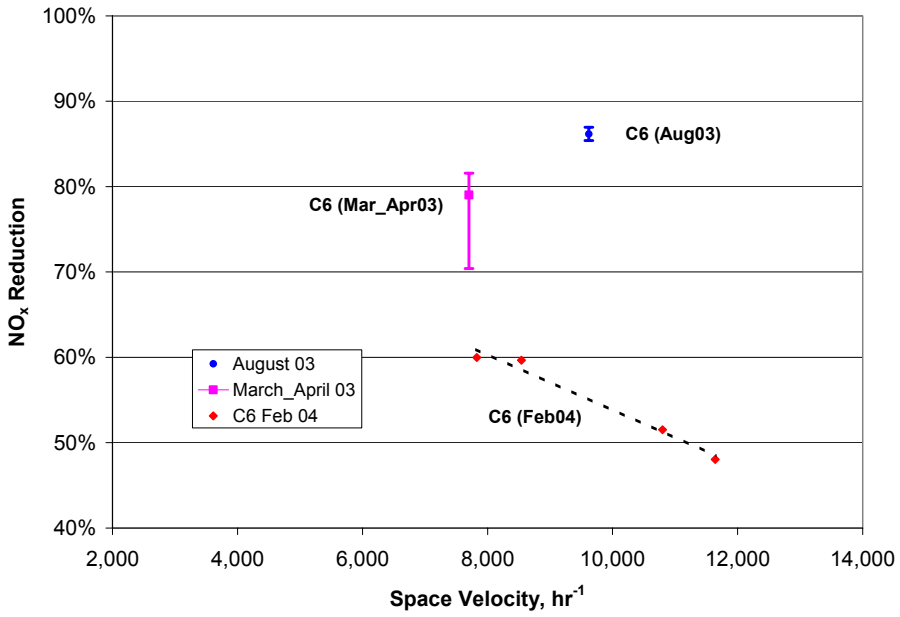

Figure 40. Catalyst activity shown as NO_x reduction as a function of space velocity for catalyst C6.

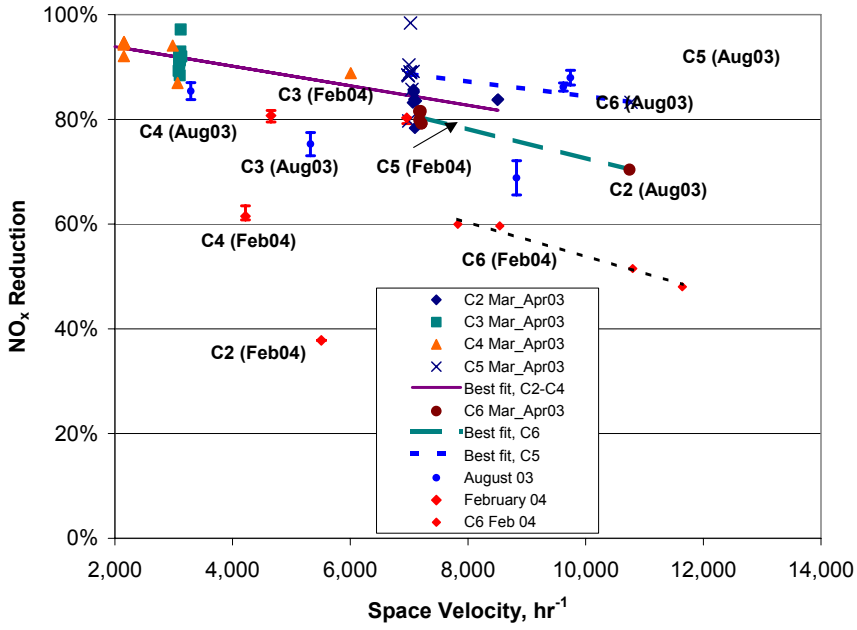

Figure 41. A general presentation of catalyst activity data for all the test catalysts. Temperature range: 653-685°F; NH_3/NO range: 0.95 – 1.29.

Problems in the Reporting Period

Eductor Plugging

The SCR slipstream reactor remained idle during the months of an outage. After the outage, flow could not be established in the reactor due to plugging of the eductors that pull flue gas through the reactor. This problem has been resolved and the reactor is operational.

Sampling Problems

Sampling problems frequently made NO_x and O_2 measurements unavailable. The problem this time has been mostly due to the plugging of the sample filters. Further, we have also experienced problems with two of the sequencer valves in the hot box. The inlet valve stays open all the time, as such while the inlet is not in use the line has to be shut manually. Valve for C6 in the sequencer fails to open. Thus sampling of line 6 involves disconnecting the sample line and connecting it to one of the other operational valves. This and other sampling problems are currently being addressed.

Field Point Module

In February, we experienced problems with the Field Point module that made it difficult to sample gases continuously over an extended period of time.

Biomass Co-firing Tests

Plans are being made to take the reactor out of service on April 30 at the Rockport plant; this corresponds to an outage at the plant.

During this quarter, inlet and outlet ports were installed at Gadsden Unit 1 for the slipstream reactor during an outage. The inlet port is at the economizer exit (Figure 42) and the outlet port is downstream of the air preheater (Figure 43).

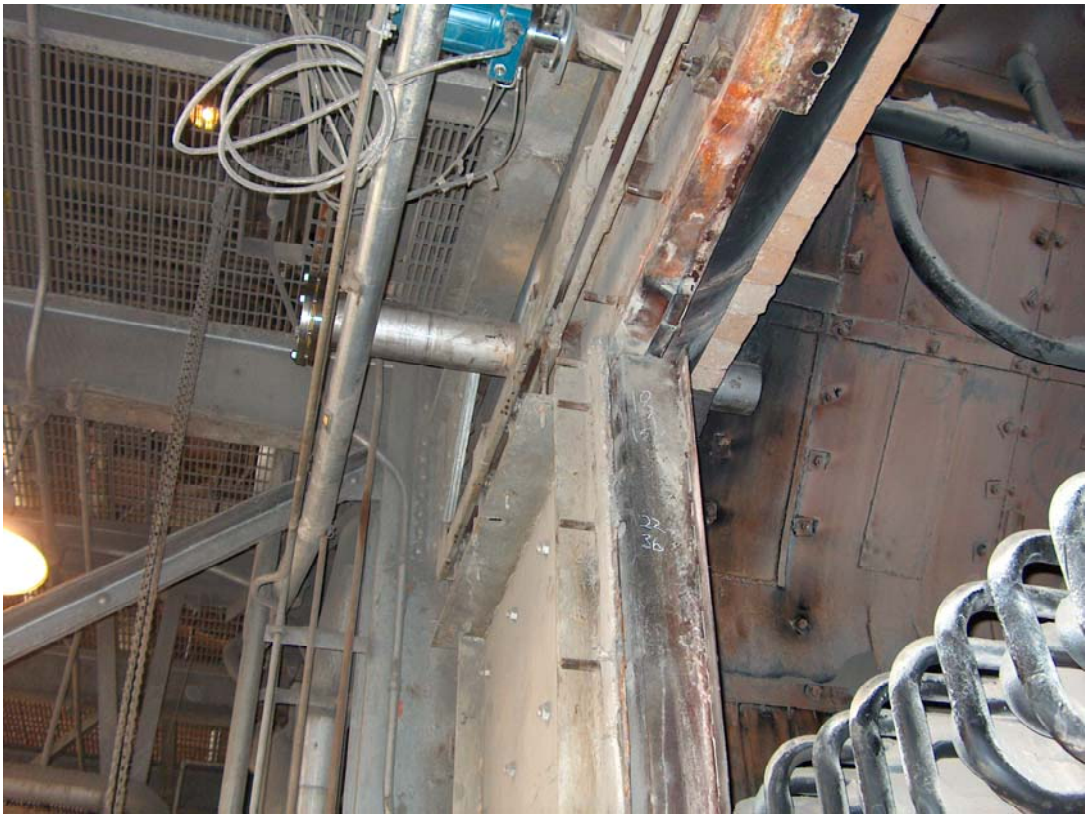

Figure 42. Inlet port installed at economizer exit at Plant Gadsden.

Figure 43. Outlet port installed at air preheater exit at Plant Gadsden.

Results and Discussion

Discussion of the Catalyst Activity Study

At this point, some significant insights can be mentioned. Only slight and statistically insignificant differences in catalyst activity between the fresh and exposed catalyst samples were observed (Figure 29), although there are obvious differences in catalyst surface composition of these samples as determined by XPS (compare Figure 32 and Figure 33). Indeed, the exposed catalyst surface contains a considerable amount of Ca and Na—the same elements that caused significant deactivation of the laboratory-poisoned catalysts. Furthermore, Na and Ca are present in large amounts as judged by the height of the Na and Ca peaks of the XPS survey scans, while the vanadium peak is not seen on either fresh or poisoned samples. It is likely that, even after fly ash removal, the overall exterior contaminant content of the catalyst greatly surpasses the near-stoichiometric Na:V or Ca:V ratios in BYU's laboratory study of catalyst poisoned by wet impregnation.

Thus, there are important differences between the wet-poison-impregnated, laboratory-prepared powdered samples and the commercial catalysts that were exposed to fly ash *in-situ*. Due to the method of poisoning of the powder samples (wet impregnation by aqueous Na or Ca salt solutions), the catalysts are uniformly poisoned through the catalyst pores, and the poisons are likely intimately bound to active Brønsted acid sites. However, even though these same elements are found in fly ash in large amounts, they do not affect the commercial catalyst to an observable extent, since apparently Na and Ca species are retained in (remain chemically bound to) the fly ash particles on the exterior catalyst surface and do not associate intimately with the active vanadium catalyst sites inside the pores of the catalyst. Any poisoning that does occur is minimal and likely limited to the surface where the solid ash resides.

These results suggest that, at least in this case, Na and Ca species do not attach to catalytically active sites through long-term exposure of commercial catalysts to ash-containing flue gas at temperatures exceeding the dew point. However, below the dew point, condensed H_2O could leach out these elements from the fly ash into the catalyst. Future work should explore this possibility. Furthermore, the field data suggest a decrease in activity of these same catalysts over the testing period. Our results suggest that this possible decrease should be attributed to fouling of the catalyst surface and not to chemical poisoning by fly ash.

Activity of catalyst M1 (C6) computed from NO_x measurements in the field at the slipstream reactor show more reduction in activity than the laboratory measurements. There are several possible reasons for this: the presence of ash deposits in the slipstream reactor, different gas compositions between the field and the laboratory or temperature differences. These questions will have to be explored more fully as the other two monolith catalysts are tested in the laboratory.

48

Conclusions

Good progress has been made on several fronts during the last three months. In particular:

- At AEP's Gavin Plant, data from the corrosion probes showed that corrosion rate increased as boiler load was increased. During an outage at the plant, the drop in boiler load, sensor temperature and corrosion rate could all be seen clearly. Restarting the boiler saw a resumption of corrosion activity. This behavior is consistent with previous observations made at a 600MWe utility boiler. More data are currently being examined for magnitudes of corrosion rates and changes in boiler operating conditions.
- There are important differences between the wet-poison-impregnated, laboratory-prepared powdered samples and the commercial catalysts that were exposed to fly ash *in-situ*. Na and Ca species do not attach to catalytically active sites through long-term exposure of commercial catalysts to ash-containing flue gas at temperatures exceeding the dew point. However, below the dew point, condensed H_2O could leach out these elements from the fly ash into the catalyst.
- Preliminary laboratory measurements at BYU of activity from one of the commercial catalysts shows little decrease in activity after 2700 hours in the field, as compared to the fresh catalysts. However, activity computed from NO^x measurements in the field at the slipstream reactor show more reduction in activity.

Plans for Next Quarter

Corrosion probe activity for the next quarter will focus on the following:

- Presentation of the corrosion measurement results at the 29th International Technical Conference on Coal Utilization & Fuel Systems (Clearwater Conference).
- Continued troubleshooting and local repair of EN modules.
- Continued analysis of data.
- Preparations for the next plant visit.

Laboratory SCR catalyst studies for the next quarter will focus on the following:

- Acidity tests on the fresh, exposed, and poisoned catalysts to determine active site density and determine how it is affected by poisons and exposure to fly ash.
- BET surface are and average pore size will be compared among catalysts.
- Further the MTR NH_3 oxidation issues and test an additional monolith catalyst at higher temperatures and in the presence of water and SO_2.

SCR slipstream activity for the next quarter will focus on the following:

- Removal of the reactor from Rockport and shipment to Plant Gadsden.
- Installation of the reactor at Plant Gadsden.

References

Busca, G., L. Lietti, et al. (1998). "Chemical and mechanistic aspects of the selective catalytic reduction of NOx by ammonia over oxide catalysts: A review." Applied Catalysis B-Environmental **18**(1-2): 1-36.

Chen, J. P., M. A. Buzanowski, et al. (1990). "Deactivation of the Vanadia Catalyst in the Selective Catalytic Reduction Process." Journal of the Air & Waste Management Association **40**(10): 1403-1409.

Chen, J. P. and R. T. Yang (1990). "Mechanism of Poisoning of the V_2O_5 TiO_2 Catalyst for the Reduction of NO by NH_3." Journal of Catalysis **125**(2): 411-420.

Orsenigo, C., L. Lietti, et al. (1998). "Dynamic investigation of the role of the surface sulfates in NO_x reduction and SO_2 oxidation over V_2O_5-WO_3/TiO_2 catalysts." Industrial & Engineering Chemistry Research **37**(6): 2350-2359.

Went, G. T., L. J. Leu, et al. (1992). "The Effects of Structure on the Catalytic Activity and Selectivity of V_2O_5/TiO_2 for the Reduction of NO by NH_3." Journal of Catalysis **134**(2): 492-505.

Appendix A:

"A Multi-point Corrosion Monitoring System Applied in a 1300 MW Coal-fired Boiler" by Kevin Davis, Temi Linjewile, David Swensen, Darrin Shino, J.J. Letcavits, William Cox, Richard Carr and N.S. Harding

Paper to be presented at the 29th Coal Utilization & Fuel Systems Conference in Clearwater, Florida, April 18-22, 2004

A Multi-point Corrosion Monitoring System Applied in a 1300 MW Coal-fired Boiler

K. A. Davis, T. M. Linjewile, J. Valentine, D. Swensen and D. Shino
Reaction Engineering International
77 West 200 South, Suite 210
Salt Lake City, Utah 84101, USA

J. J. Letcavits, R. Sheidler
American Electric Power Company, Inc.
1 Riverside Plaza, Columbus, Ohio 43215-2373

W. M. Cox and R. N. Carr
Corrosion Management Engineering Consultants
First House, Spring Avenue
Hyde, Cheshire SK14 5LT, United Kingdom

N. S. Harding
N.S. Harding & Associates
1019 East Eaglewood Drive
North Salt Lake, Utah 84054, USA

ABSTRACT

Combustion modifications to minimize NOx emissions have magnified the importance of waterwall corrosion in coal-fired boilers. As evolving regulations required further NOx emissions reduction, a cost effective approach to satisfying these requirements has been to increase the degree of air staging. However, in many applications, corrosion concerns prevent the use of such fuel rich conditions. The physics and chemistry controlling corrosion processes can be highly non-linear and are challenging to describe in terms of their likely overall combustion behavior. Therefore, decisions involving operating conditions and the selection of coal, combustion equipment and waterwall protection often have been made in a conservative and less than optimal manner. This paper describes the application of a multi-point, real-time corrosion surveillance system to a large boiler firing high sulfur coal. This technology, incorporating electrochemical sensing and wireless signal transmission, enables combustion engineers and plant operating personnel to make informed decisions regarding the quantitative relationships between operating conditions, NOx emissions, and any resultant extent/magnitude of waterwall corrosion.

INTRODUCTION

Combustion modifications, including low-NO_X burners (LNBs) and over-fire air (OFA) have proven to be the more cost-effective solutions for minimization of NO_X emissions. However, this approach often leads to the existence of reducing conditions and flame impingement on waterwalls. As regulations demand lower NO_X levels, one option is to address the requirements with increased levels of air staging. However, in most practical situations, a number of adverse impacts prevent the application of very deep staging. One of the more significant limitations is the increased corrosion that can occur on waterwall tubes exposed to fuel-rich, or alternately fuel-rich and oxygen-rich, combustion environments that are

experienced by the boiler during normal changes in operation or unit load. In utility boilers, for example, staging has increased the frequency and severity of waterwall wastage, with tube wall loss rates that can exceed 2.5 mm/yr (100 mils/yr) in some units. The industry-wide significance of this problem is pointed out by EPRI estimates indicating that fireside corrosion costs the U.S. electric power industry up to $590 million per year and is the cause of approximately half of the forced outages in steam generating plants [1]. The susceptibility of coal-fired boilers to corrosion has been related to several issues including fuel selection, tube temperature, and firing system design. Formulating solutions to this problem can be complicated by the range of potential mechanisms, which can involve gas-phase sulfur and/or chlorine contents in addition to the direct deposition of unreacted fuel and molten ash. In addition, the physics and chemistry controlling corrosion processes can be highly non-linear. Therefore, brief periods of exposure to unusual conditions can dominate the overall rate of material loss between tube inspections.

Boiler corrosion monitoring strategies commonly rely on ultrasonic tube-wall thickness measurements typically conducted at 12 to 24 month intervals during scheduled outages. Corrosion coupons are also sometimes used. These approaches require a considerable exposure time to provide meaningful data. The major drawback of such methods is that corrosion information is obtained after the damage has already been done. Management of boiler waterwall loss and system optimization therefore requires a real-time indication of corrosion rate in susceptible regions of the furnace. This paper describes preliminary results of a program of field investigations and considers the use of on-line sensing instrumentation in combination with innovative applications of CFD modeling, precision metrology and non-active corrosion coupons to allow combustion engineers and plant operating personnel to manage waterwall loss in fossil-fueled boilers while minimizing NO_X emissions.

TECHNICAL APPROACH

The availability of practical tools for analysing corrosion in a coal-fired boiler is limited. Waterwall corrosion is highly dependent upon local waterwall conditions and their relationship to fuel properties, operating conditions, and boiler/firing system configuration. Therefore the development of a predictive approach requires a 3D, two-phase computational fluid dynamics (CFD) model that incorporates relationships between corrosion rates and these local conditions. Although there are no broadly accepted correlations, several useful relationships have been identified.

On-line high-temperature electrochemical sensing is a developing technology. As real-time monitoring options have not achieved industry-wide acceptance, it is important that any surveillance technology used be verified against physical measurements during a period of stable operation. As boilers are rarely operated in a stable manner for an extended period (e.g. due to load variation, fuel property variation, and operator tendencies), it was considered useful that such checks might be undertaken during a period as short as a single operator's shift. With these concepts in mind, the present investigation combined the application of CFD tools with field instrumentation in a complementary approach to combustion optimization and tube condition management.

CFD Modeling and Corrosion Rates

Furnace tube damage can be difficult to diagnose and awkward to counter in a timely manner. However, computational simulations can provide insight into the factors controlling the nature of flow, temperature, and composition fields within a boiler.

The predictive modeling tool discussed herein is based on the CFD code *GLACIER*, which is tailored for reacting, two-phase flow systems. The approach to modeling fuel/ash particles provides a convenient basis for implementing descriptions of phenomena such as deposition and corrosion. The mean path and dispersion of an ensemble of particles, referred to as a "particle cloud," are tracked in a Lagrangian

reference frame. Dispersion of the cloud is determined with input from the turbulent gas flow field. Particle mass, momentum, and energy sources are coupled to the gas flow field through a particle-source-in-cell technique [2]. Particle reaction processes include coal devolatilization, char oxidation, and liquid evaporation. Waterwall deposition is accounted for by evaluating particle/wall interactions.

Boiler tube degradation rates can be predicted using *GLACIER* in conjunction with empirical correlations relating corrosion attack and predicted combustion properties of the boiler. Although the mechanisms responsible for the corrosion of furnace waterwall tubes are still contentious, recent work indicates that there are three primary mechanisms for waterwall wastage in U.S. coal-fired boilers [3]:

- Gas-phase attack by reduced sulfur species such as H_2S
- Deposition of unreacted fuel and resulting sulfur-based attack
- Chlorine-based attack

The details of these mechanisms are topics of active discussion. However, laboratory, pilot-scale and full-scale work have been performed from which specific correlations have been developed for each of these mechanisms. In addition, Reaction Engineering International and EPRI have applied these correlations within CFD simulations for a number of utility boilers and, with little modification to the correlations, have been able to demonstrate effectively their usefulness, based on field observations [3]. In general terms, the CFD-based effort illustrates that the approach can deliver very good agreement between predicted and observed corrosion behavior. CFD predictions for unburned material in the deposits and the corrosion rate for the south and north walls of the test boiler are shown in Figures 1a and 1b. The corresponding distribution of ultrasonic tube-wall thickness measurements for the same south wall are shown in Figure 2. The locations of the electrochemical sensors also are shown on this Figure.

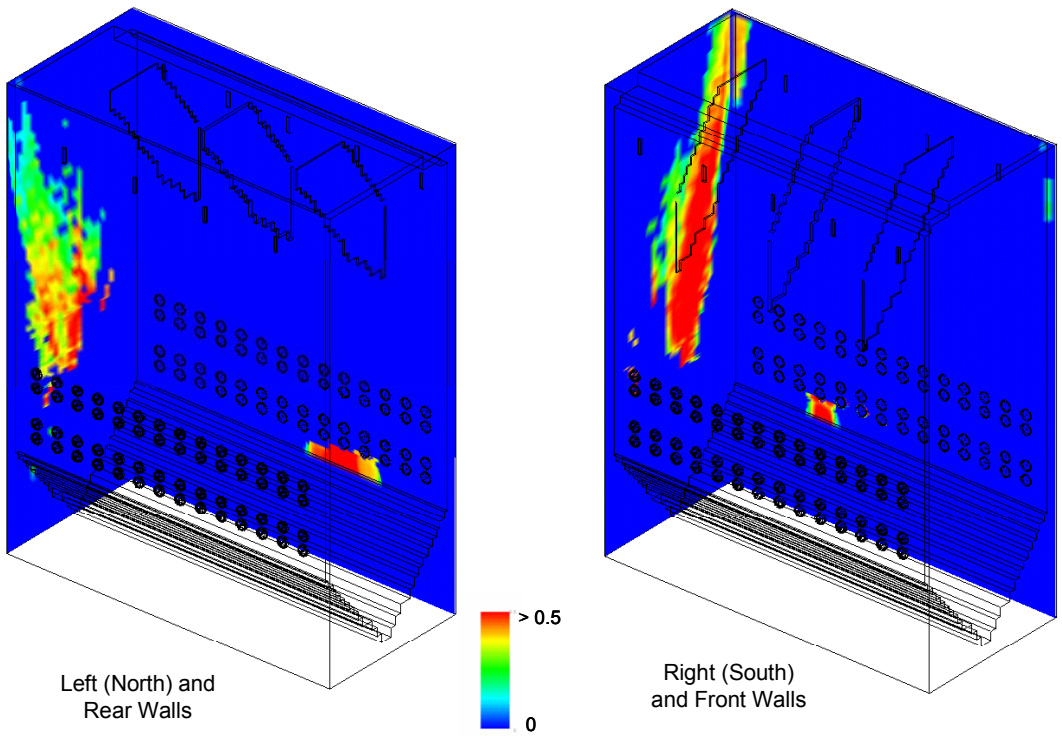

Figure 1 a. Fraction of unburned material in the deposits viewing from outside the boiler.

A preliminary analysis of the CFD results shows a clear qualitative agreement with the UT data. Further, both the CFD predictions and the UT data were in qualitative agreement with the on-line corrosion rates, which indicated that a substantially higher rate of attack occurred at the Main Probe location than was the case at the Probe 2 location. The work reported here is ongoing and further comparisons between the electrochemical sensors, surface profilometric measurements and screw-in type corrosion coupons are to be made. The CFD simulations predicted the corrosion behavior in the boiler with remarkable accuracy, and provided much information relating to the rate of attack on waterwalls. The approach is to be used to investigate strategies to mitigate attack and to determine optimal operating conditions, fuel selection, and maintenance approaches.

Probe Installation Procedures

Schedules required that ports be installed during a unit outage well before sensor probes were available. In consequence, after remaining idle for several months, the probe ports filled with deposits comprising unburned carbon, ash, solidified and semi-molten slag on the waterwall fireside. The ports had to be cleaned to permit installation of the probes. Figure 3 shows a picture of a probe port before and after cleaning. Six electrochemical sensors were prepared for installation. The probe locations were chosen on the basis of prior knowledge of plant corrosion behavior. One probe was installed on the North Side Wall and five were designated for installation on the South Side Wall, as shown schematically in Figure 4, as it was known that corrosion attack was more prevalent on the South waterwall. Alongside each of the electrochemical sensors, three "KEMKOP" type screw-in corrosion coupons were installed. The procedure for installing the electrochemical sensors involved gradually advancing the probes into the furnace to allow for thermal equilibration. The probes were positioned such that the sensor face was located at the crown of the adjacent tubes.

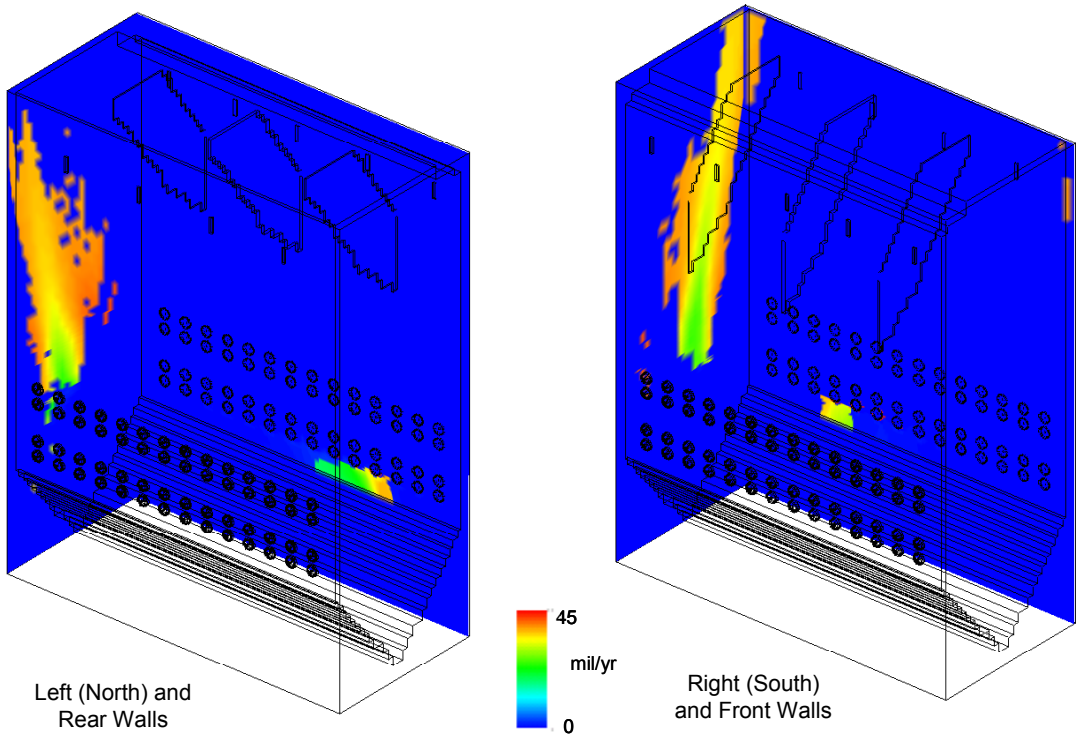

Figure 1 b. CFD Predictions of corrosion rate in the north and south walls.

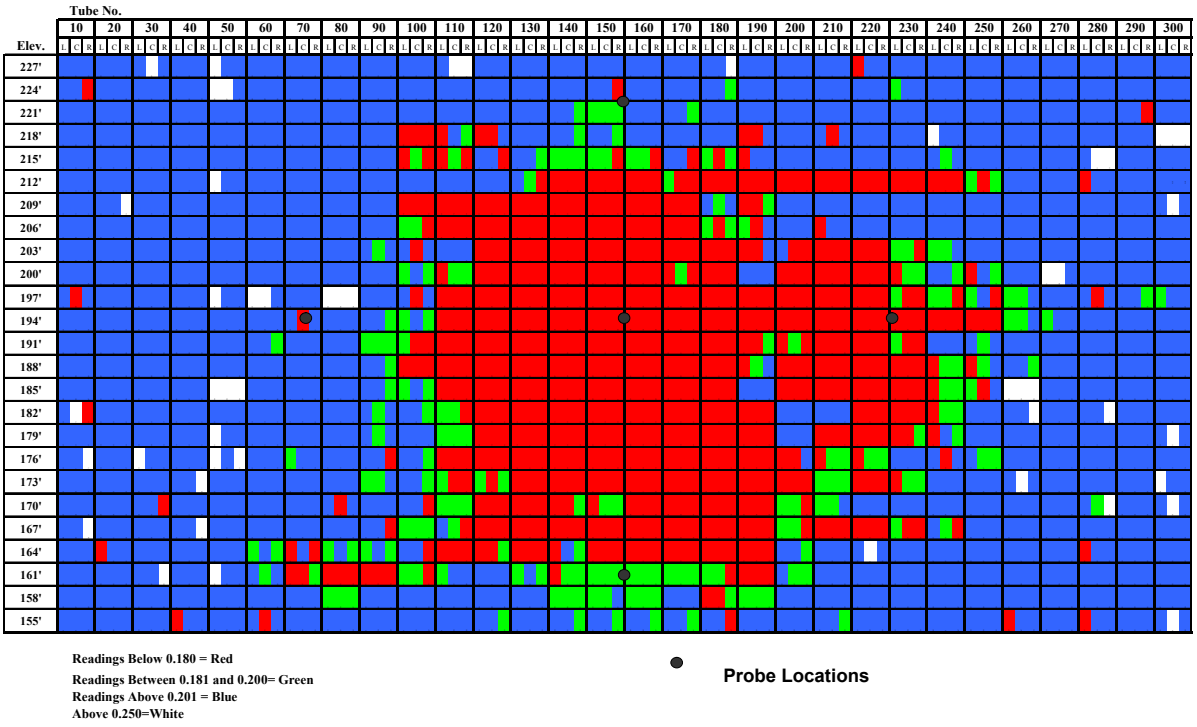

Figure 2. UT map of the south wall showing high corrosion areas in red and low corrosion areas in blue and white.

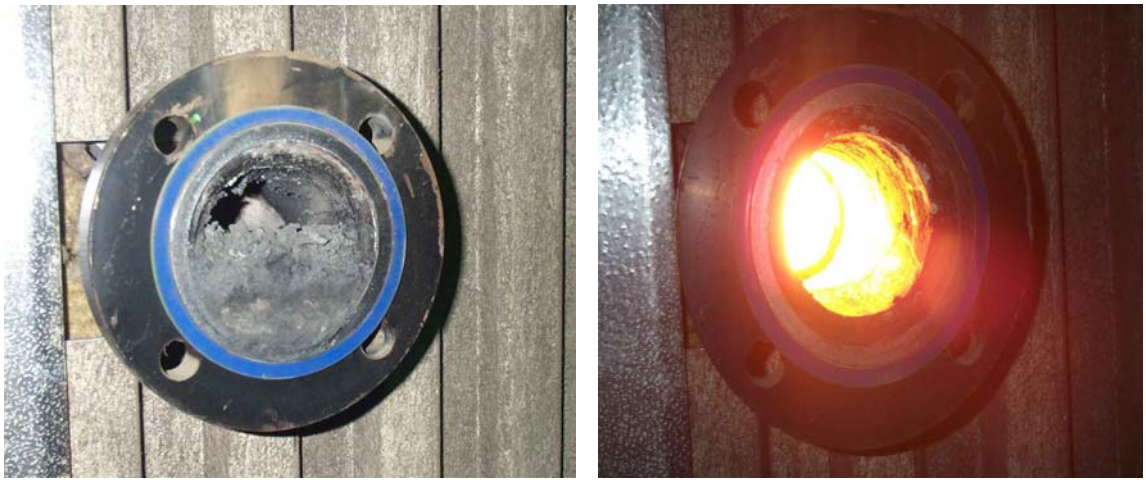

Figure 3. Appearance of a probe port before (left) and after cleaning (right).

Figure 5 shows a fully installed probe, and a covered rectangular port, adjacent to the electrochemical sensor into which KEMKOP coupons were located. Figure 6 shows the control layout for the multi-probe installation. Six control boxes were used, five of which were located on the south wall side and one was

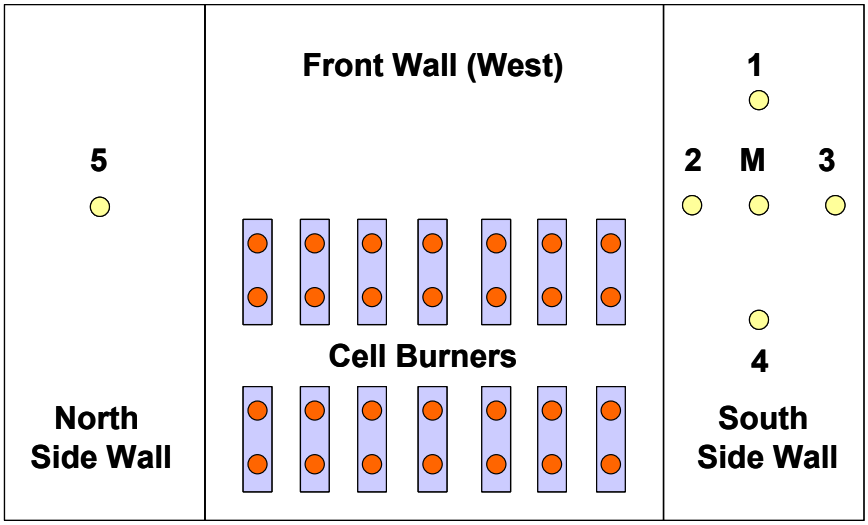

Figure 4. Location of corrosion sensors viewed from outside the boiler.

Figure 5. Corrosion sensor installed at location 2 on the south wall.

located on the north wall side. The south wall held the center probe and Probes 1 to 4. The center probe was designated as the Main Probe for convenience, as its control electronics were housed in the Main Control box. The probe located on the north wall was designated as Probe Number 5.

While a probe is coming to the boiler waterwall temperature set point, data are collected. However, these data points are not analyzed. Once the face temperature is maintained, the electrochemical data are recorded and plotted. The clock time was noted and control room data and probe data were recorded.

.

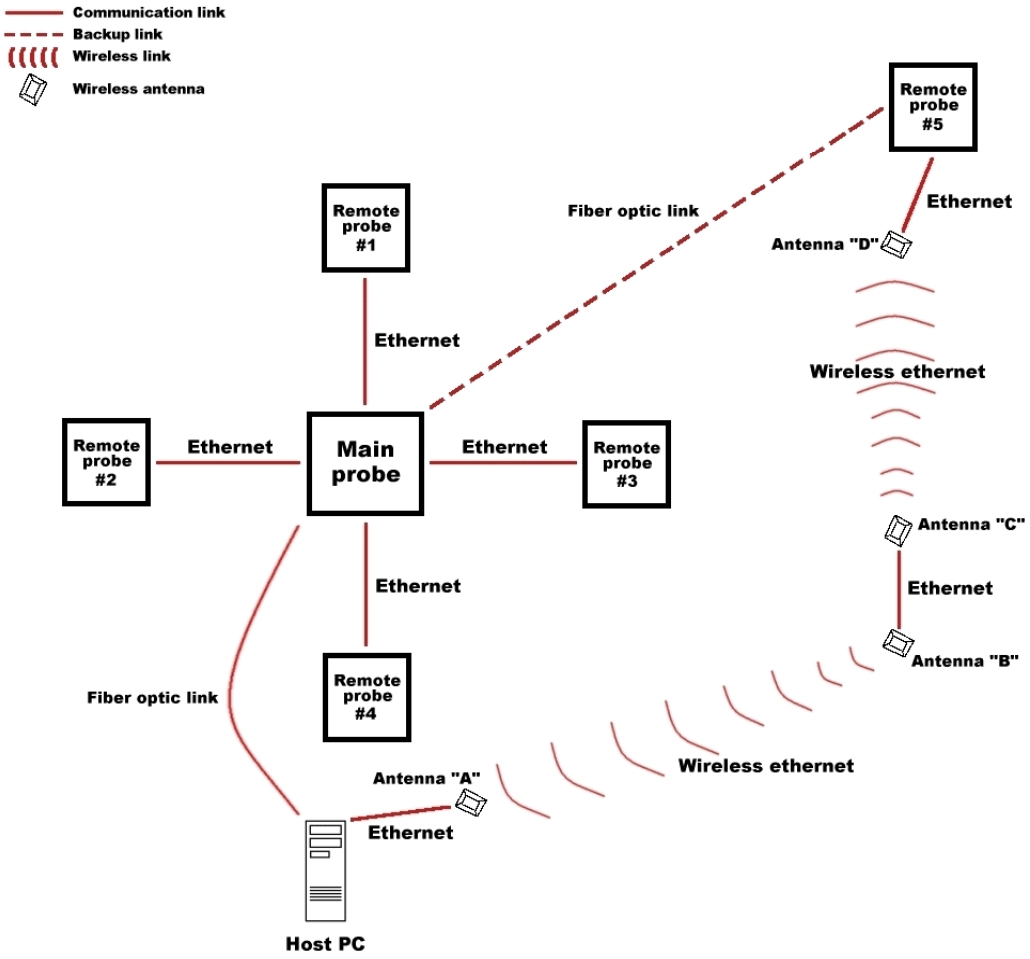

Figure 6. Schematic diagram of the multi-sensor communication and control layout.

Fundamental Description

The fluctuation in the potential signal measured is referred to as electrochemical potential noise (EPN) and the fluctuation in current is defined as electrochemical current noise (ECN). These were used for calculating the noise resistance (R_n). Corrosion current, I_{Corr}, is calculated by replacing the polarization resistance (R_p) in the Stern-Geary equation with the noise resistance, (R_n).

$$I_{Corr} = \frac{B}{R_n}$$

where B is the Stern-Geary coefficient. A detailed description of the fundamental principles of electrochemical noise for corrosion measurement can be found in Hladky [4], Syrett and Cox [5], Cottis and Turgoose [6].

RESULTS AND DISCUSSION

During the past two decades, efforts have been made to apply real-time corrosion monitoring technologies and evaluate/develop their usefulness in high temperature combustion environments. Although these

adaptations have had some success in certain industries [7], tests in other areas, such as utility boilers, have been met with skepticism. Nonetheless, an evaluation of available technologies and advances in measurement techniques conducted by REI identified electrochemical noise monitoring technology as a promising option for further development and evaluation [8].

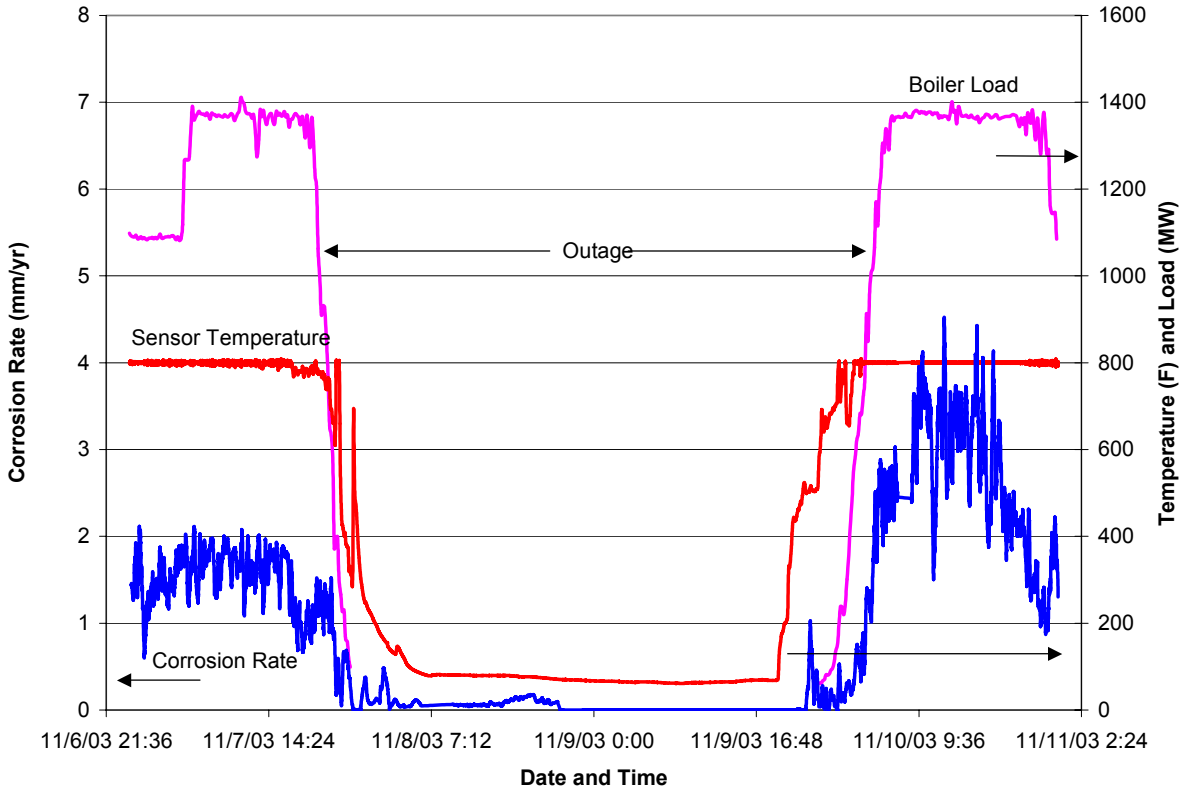

Figure 7. Electrochemical noise sensor response (Main Probe) to a decreasing and increasing load before and after an outage.

Effect of Boiler Load on Corrosion Rate

Plant tests were conducted at a 1300 MWe supercritical boiler. The response of the corrosion sensor at the center of the south wall (Main Probe) of the boiler before and after an outage is shown in Figure 7. The graph shows corrosion rate, boiler load and the sensor temperature trace as a function of boiler operating time. As the boiler load increased there was a corresponding increase in the observed corrosion rate. The boiler load then stabilized, causing the probe also to maintain a stable corrosion rate, which was interrupted from time to time by changes in local conditions, even at constant boiler load. The ensuing decrease in boiler load, sensor temperature and corrosion rate occurred with load reduction going into an outage. It may be noted that, just prior to load reduction, the sensor temperature decreased, causing the corrosion rate also to fall. Restarting the boiler saw a resumption of corrosion activity. The right hand side corner of Figure 7 shows the Main Probe response as the boiler load was ramped up. Clearly, corrosion rate increased as boiler load was increased and then briefly remained stable. Thereafter, the corrosion rate decreased even as the boiler load and sensor temperature remained constant, an indication of the sensor's responsiveness to local boiler conditions.

Effect of Local Waterwall Conditions

Local waterwall corrosion may vary, depending upon whether reducing, oxidizing, or fluctuating reducing and oxidizing conditions are prevalent. The local corrosion behavior also can be influenced by ash and slag deposition. A comparison of the summary of daily average corrosion rates for Probe 2 and the Main Probe for the period of October 25 to November 29, 2003 is shown in Figure 8. The graph shows that during normal boiler operation, corrosion rates at the two locations were quite different, indicating that the local conditions in these two probe sites also were different. Further analysis of corrosion rate records for the three locations (see Figure 9) revealed that lower corrosion rates occurred at Probe 2 and Probe 3 than was the case at the Main Probe location. The corrosion rates measured at Probe 2 and the Main Probe were consistent with ultrasonic tube-wall thickness measurements (UT) that had been obtained prior to sensor installation.

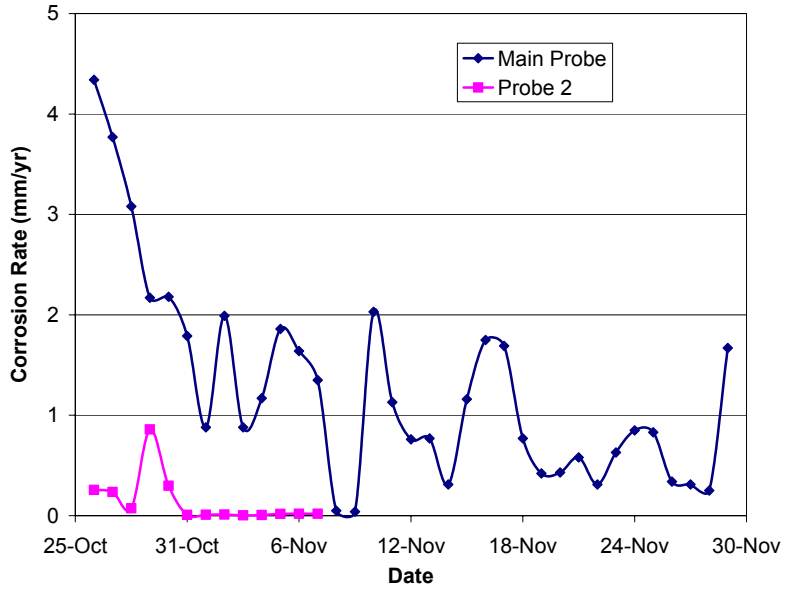

Figure 8. Daily average corrosion rate for the Main Probe and Probe 2 during the period of October 26 to November 29, 2003.

Corrosion Rate and Ash Deposition

After three months of testing, the probes were removed from the plant and a record of the appearance of the probe ports and the sensor heads was taken. Upon retrieval of the Main Probe, the port was clear and unobstructed. The left hand side of Figure 10 shows the corrosion probe head covered with a layer of solidified molten slag. Given the clear and clean conditions of the port it was envisaged that the molten slag solidified during probe retrieval as the sensor cooled. The slag layer on the Main Probe broke-off easily. Further observation of the sensor face after the slag layer was broken off revealed presence of dark-colored deposits (possibly unburned carbon or magnetite), an indication of the presence of reducing conditions in the vicinity of the Main Probe location. The right hand side of Figure 10 shows the sensor face after the slag layer was broken away.

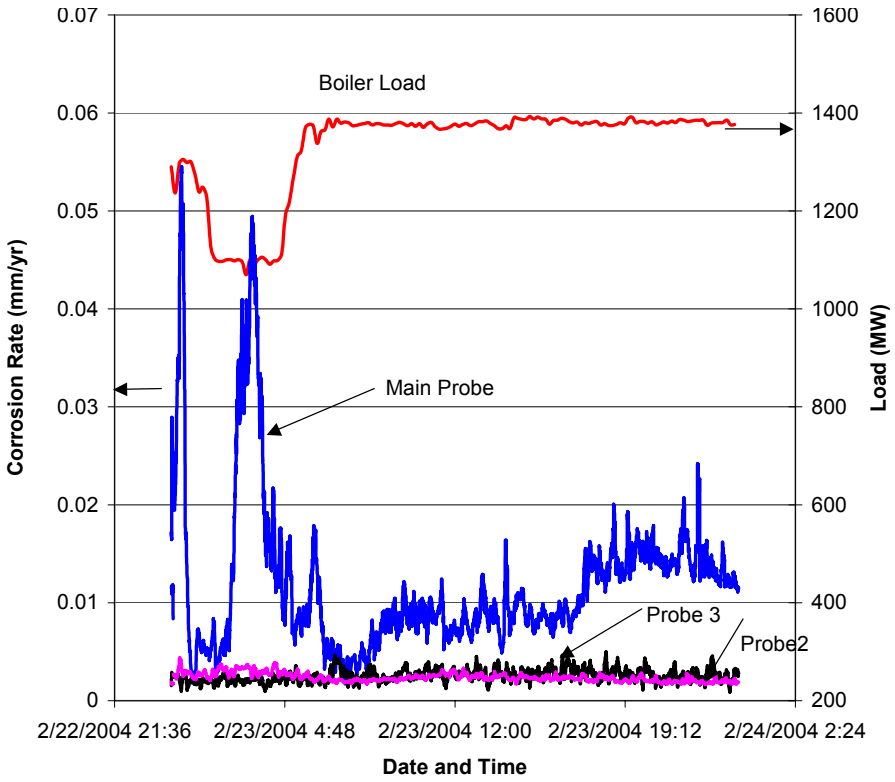

Figure 9. A snapshot of corrosion rates at three probe locations

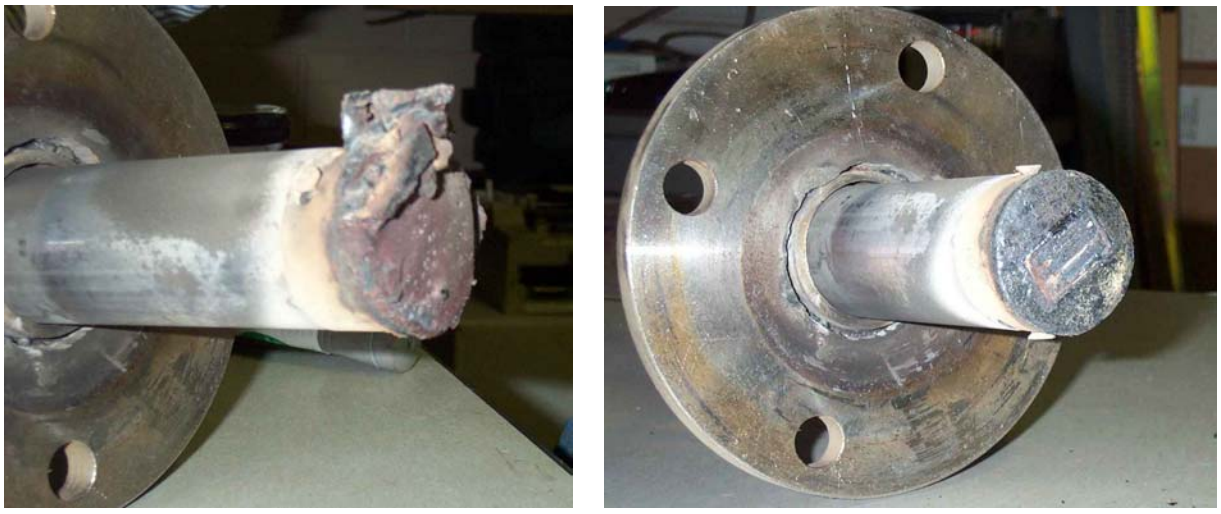

Figure 10. Main Probe covered by a layer of slag (left) and sensor face after removal of the slag layer.

By contrast, a layer of solidified slag shown in the left hand side part of Figure 11 covered the inner opening of probe port 2. In addition Probe 2 (Right hand side of Figure 11) was not covered by a layer of molten slag, as was the case with the Main Probe. The layer of light deposit on Probe 2 was red in color, suggesting the presence of hematite, which is an indication that oxidizing conditions probably prevailed at probe location 2. Optical pyrometer temperature measurements that were taken after retrieving the probes showed that the temperature at the Probe 2 port location was approximately 2580°F and that the temperature at the Main Probe location was 2450°F. However, reducing and oxidizing conditions may have influenced the state of the slag at both probe locations. Reducing conditions lower the melting point of slag, thereby helping to maintain a liquid slag at the Main Probe location. Oxidizing conditions may have maintained a semi-molten slag at the Probe 2 port location. Further, the presence of molten slag may have facilitated corrosion by dissolution of iron into the slag melt.

Figure 11. Probe port 2 after removal of the EN sensor (left) and appearance of the sensor elements (right).

CONCLUSIONS

The results of this investigation indicate that electrochemical sensors can provide qualitative and quantitative descriptions of high temperature corrosion conditions in the radiant section of utility boilers. However, the complex relationship between corrosion and fuel properties, firing systems, and operating conditions in a coal-fired boiler can make it difficult to predict, diagnose, and manage waterwall wastage. It is therefore important to utilize a combination of tools to obtain maximum control and service life predictability. Three promising technologies have been identified that can be used in a complementary manner to provide a highly effective approach. Application of these tools may vary, based on the needs of a particular situation, but in general the approach could include the following steps:

- Evaluate historical records and available fuel analyses, deposit analyses, tube temperature measurements, and heat flux measurements to identify potential corrosion mechanisms in a boiler or furnace.

- Conduct CFD simulation of the boiler over a range of relevant conditions to identify areas susceptible to deposition of unoxidized material and corrosion.

- A comparison of CFD results and plant observations, including ultrasonic tube wall thickness measurement data and tube failure information, can be used to build confidence in the model

inputs, predict likely trouble spots and key fuel properties, initiate combustion modifications (i.e. LNBS and OFA), and identify optimal operating conditions.

- The installation of real-time electrochemical sensors, whether single or multiple configurations can be optimized by plant observations and CFD modeling results and is a low-cost method of maintaining a continuous management of the service environment.

- The approach is easy to validate for quantitative accuracy by means of precision metrology.

- CFD modeling can be used to develop guidelines for optimizing the boiler, based on plant-specific considerations including NO_X emissions, carbon-in-fly ash, and waterwall wastage.

- The use of real-time sensor(s) facilitates close management of waterwall wastage because the operating conditions can be used to optimize the commercial dispatch of the unit.

- Real-time sensing of tube wall corrosion rates as a function of unit operation allows timely and effective remedial action to be taken to avoid unnecessary damage, reduce outage times and avoid unexpected maintenance. .

ACKNOWLEDGEMENTS

Funding for this effort was provided by the Ohio Coal Development Office through contract CDO/D-01-15 under the supervision of Howard Johnson and the Department of Energy /NETL through contract DE-FC26-00NT40753 under the supervision of Bruce Lani. Funding for the corrosion-specific aspects of the CFD and installation of the KEMA screw-in type corrosion coupons was provided by EPRI with technical guidance from and under the supervision of Wate Bakker and Tony Facchiano. The authors are grateful to Fred Wheeler at AEP Gavin Station for providing technical assistance on site and to Dana Overacker for technical assistance in fabrication of the corrosion sensors at the University of Utah.

REFERENCES

1. Syrett, B. C. and Gorman, J. A., “Cost of Corrosion in the Electric Power Industry – An Update”, *Materials Performance*, **42** (2), 32-38, 2003.
2. Crowe, C. T., Sharma, M. D., and Stock, D. E., *J. Fluids Eng.* 1977, **99**: 325.
3. EPRI, Waterwall Wastage Mechanisms in Coal-fired Boilers: The effect of Coal Chemistry on Waterwall Wastage, TR-1004021, Palo Alto, CA 2001.
4. Hladky, K., US Patent 4575678.
5. Syrett, B. C., and Cox, W. M., “A Review of EPRI Projects Since 1984 that Used Electrochemical Noise Instrumentation,” in Electrochemical Noise Measurement for Corrosion Applications STP 1277, Jeffrey R. Kearns, John R. Scully, Pierre R. Roberge, David L. Reichert, and John Dawson, Eds., ASTM 1996, 173-185.
6. Cottis, R., and Turgoose, S., “Electrochemical Impedance and Noise,” in Corrosion Testing Made Easy, Barry C. Syrett, Series Editor, NACE International, 1999.
7. Kane, R. D., and Cayard, M. S., Chemical Engineering Progress, 1998; 94: 49.
8. Davis, K., Lee, C., Seeley, R., Harding, S., Heap, M., Cox, W., *25th International Technical Conference on Coal Utilization & Fuel Systems*, Clearwater, FL, March 2000.